A HANDBOOK OF DETERMINATIVE METHODS IN CLAY MINERALOGY: TRANSMISSION ELECTRON MICROSCOPY

Chapter · December 1987

CITATIONS
5

READS
497

2 authors, including:

P H Nadeau
University of Stavanger (UiS)
111 PUBLICATIONS **3,128** CITATIONS

SEE PROFILE

A HANDBOOK OF DETERMINATIVE METHODS IN CLAY MINERALOGY

Edited by
M.J. WILSON
Head, Department of Mineral Soils
Macaulay Institute for Soil Research
Aberdeen

Blackie
Glasgow and London

Published in the USA by
Chapman and Hall
New York

Blackie & Son Limited,
Bishopbriggs, Glasgow G64 2NZ
7 Leicester Place
London WC2H 7BP

Published in the USA by
Chapman and Hall
in association with Methuen, Inc.
29 West 35th Street, New York, NY 10001-2291

First published 1987

British Library Cataloguing in Publication Data

A Handbook of determinative methods in clay mineralogy.
1. Clay minerals
I. Wilson, M.J.
549'.67 QE389.625

ISBN 0-216-91801-4

Library of Congress Cataloging-in-Publication Data

A Handbook of determinative methods in clay mineralogy.

Includes bibliographies and index.
1. Clay—Analysis. 2. Mineralogy, Determinative.
I. Wilson, M. J. (Michael John), 1939–
QE471.3.H36 1987 549'.6 87-11714
ISBN 0-412-00901-3 (Chapman and Hall)

Phototypesetting by Thomson Press (I) Ltd., New Delhi
Printed in Great Britain by Bell & Bain (Glasgow) Ltd.

Preface

This book emerged gradually from discussions on clay mineralogy with visiting scientists at the Macaulay Institute. It was realized that to many such scientists clay mineralogy was a vital, but peripheral, component of their work, yet they were often in the position of having to study clay mineralogy from scratch. It became apparent that there was a need for an introductory text covering practical aspects of the main investigative methods in clay research. At the same time, such a text could also provide a useful compilation for scientists already familiar with the difficulties of investigating clay minerals.

All but one of the contributors to this book are, or have been, associated with the Macaulay Institute. The Institute has a long and distinguished history of research into clay mineralogy and has numbered on its staff such eminent figures as D.M.C. MacEwan, G.F. Walker, V.C. Farmer and R.C. Mackenzie. Special mention must be made of Dr Mackenzie, however, because he fully appreciated the complex nature of clays, and was instrumental in initiating and encouraging a multi-technique approach in the characterization of these materials at the Institute. In a very real sense this book is a tribute to his work.

Special thanks are due to the technical staff of the Institute who, in uncertain circumstances, did a magnificent job in providing much of the original material on which this book is based. In particular the authors are indebted to D.M.L. Duthie, D.R. Clark and Mrs L. Forsyth (X-ray diffraction), Miss J.L. Bunch and Miss C.J. Bruce (thermal analysis), A.R. Fraser and I. Black (infrared spectroscopy), Miss L. Mielewczyk (electron microscopy), Miss S. Buchan (chemical analysis) and Mrs S. Ritchie and Miss M. Thom (selective dissolution methods). We are also grateful to the Director, Professor T.S. West, for allowing us to undertake and complete this book with the minimum of formalities, and to Miss Y. Bisset for the not inconsiderable labour of typing the manuscript.

MJW

Contributors

D. C. Bain, Macaulay Land Use Research Institute, Craigiebuckler, Aberdeen AB9 2QJ, UK.

A. C. Birnie, Macaulay Land Use Research Institute, Craigiebuckler, Aberdeen AB9 2QJ, UK.

P. L. Hall, Schlumberger, PO Box 153, Cambridge CB2 3BE, UK.

W. J. McHardy, Macaulay Land Use Research Institute, Craigiebuckler, Aberdeen AB9 2QJ, UK.

B. D. Mitchell, Macaulay Land Use Research Institute, Craigiebuckler, Aberdeen AB9 2QJ.

P. H. Nadeau, Statoil, Forus, Postboks 300, Stavanger, N-4001 Norway.

E. Paterson, Macaulay Land Use Research Institute, Craigiebuckler, Aberdeen AB9 2QJ, UK.

J. D. Russell, Macaulay Land Use Research Institute, Craigiebuckler, Aberdeen AB9 2QJ, UK.

B. F. L. Smith, Macaulay Land Use Research Institute, Craigiebuckler, Aberdeen AB9 2QJ, UK.

R. Swaffield, Macaulay Land Use Research Institute, Craigiebuckler, Aberdeen AB9 2QJ, UK.

J. M. Tait, 9 Papdale Road, Kirkwall, Orkney KW15 1JT, UK.

M. J. Wilson, Macaulay Land Use Research Institute, Craigiebuckler, Aberdeen AB9 2QJ, UK.

Contents

1 Clays: their significance, properties, origins and uses

P.L. HALL

1.1 Introduction

To most of us the word 'clay' usually means a fine-grained material which when mixed with water becomes extremely plastic and mouldable. Yet clays have a much wider impact on our lives than many of us commonly realize. They form an important constituent of soils, where they exert a dominant influence on soil structure and plant nutrition. Clays are used for brick-making, as fillers and coating agents in paper manufacture, and of course in ceramics. Their properties are complex and of great scientific interest, as indicated by the enormous amount of research on clays which has been undertaken by geologists, mineralogists, chemists, engineers and others over a considerable period of time. In this chapter, an introduction is given to the nature of clays and their fundamental properties, how they occur and are formed in nature, and some ideas of their use and importance.

The term 'clay' is often (e.g. in soil mechanics) used in the restricted sense of a particle-size classification term for the natural constituents of soils and sediments. In this usage, clays describe a chemically very heterogeneous and structurally complex assemblage of colloidal particles, having mean diameters ranging from a few microns (μm) down to a few hundredths of a micron (a micron is one thousandth of a millimetre). Chemically, this complex assemblage consists of a considerable quantity of hydrous aluminium silicates, with lesser amounts of finely divided quartz, feldspars, carbonates, oxides and hydroxides (mainly of aluminium and iron) and organic matter. 'Clay minerals' refers collectively to the group of fine-grained hydrous silicates of aluminium (and also to some extent of magnesium or iron). When examined under the scanning electron microscope, these minerals are seen to consist of readily identifiable particles, which can have a variety of geometric shapes (flat or crinkly plates, ribbons, tubes or pods). Despite this variety of morphology, clays are closely interrelated in terms of their basic crystal structures, and also in the characteristic physical and chemical properties resulting from their crystal chemistry.

Smart, P. and Tovey, N.K. (1981) *Electron Microscopy of Soils and Sediments: Examples.* Clarendon Press, Oxford, 178pp.
Smart, P. and Tovey, N.K. (1982) *Electron Microscopy of Soils and Sediments: Techniques.* Clarendon Press, Oxford, 400pp.
Springer, G. (1974) The role of carbon film thickness in electron microprobe analysis: a comment. *Am. Miner.*, **59**, 1121–1122.
Statham, P.J. (1979) Measurement and use of peak-to-background ratios in X-ray analysis. *Mikrochimica Acta. Suppl.*, **8**, 229–242.
Sweatman and Long, (1969) Quantitative electron-probe microanalysis of rock-forming minerals. *J. Petrol.*, **10(2)**, 332–379.
Swift, J.A. and Brown, A.C. (1979) SEM electron source: pointed tungsten filaments with long life and high brightness.
Tait, J.M., Violante, P. and Violante, A. (1983) Co-crystallization of gibbsite and bayerite with norstrandite. *Clay Miner.*, **18**, 95–99.
Tazaki, K. (1979) 'Micromorphology of halloysite produced by weathering plagioclase in volcanic ash,' in *Proc. VI Intern. Clay Conf. 1978.* (M.M. Mortland and V.C. Farmer eds.) Elsevier, Amsterdam, 415–422.
Velde, B. (1984) Electron microprobe analysis of clay minerals. *Clay Miner.*, **19**, 243–247.
White, G.N., Berkheiser, V.E., Blanchard, F.N. and Hallmark, C.T. (1982) Thin-film analysis of clay particles using energy dispersive X-ray analysis. *Clays & Clay Miner.*, **30(5)**, 373–382.

6 Transmission electron microscopy

P.H. NADEAU AND J.M. TAIT

6.1 Introduction

6.1.1 *General statement*

The transmission electron microscope (TEM) is a high-resolution instrument which provides information concerning the sizes and shapes of clay particles and aggregates. Clay materials are well suited for examination by TEM, because most specimens are composed of particles with planar dimensions 10 to 10^3 nm within the optimum operating magnification range, (10^3 to 10^5), of these instruments. The construction of the microscope is analogous to the conventional optical microscope (Figure 6.1), but the electrons provide the illumination and electromagnetic 'lenses' condense the electron beam and magnify the specimen image. The strong interactions between electrons and matter require a high-vacuum environment (10^{-2}–10^{-4} Torr) in the microscope column, ultrathin specimen support films (1–10 nm) and thin specimens (< 100 nm). The instrument can also be operated in a diffraction mode, producing electron-diffraction (ED) patterns which are useful in determining the crystalline nature of clay particles and aggregates. Some instruments are also fitted with analytical systems which can determine the chemical composition of the specimen. Thus, the characterization of materials by TEM provides valuable information concerning the size, shape, structure and composition of clay particles on a scale which is not approachable by other analytical techniques.

6.1.2 *Historical development*

The first electron micrographs of clay materials were published by W. Eitel and his associates in 1940, these early studies being primarily concerned with the size and morphology of kaolinite and montmorillonite. The fibrous morphology of palygorskite (attapulgite) was observed by other workers in 1942, and the tubular nature of chrysotile and halloysite in 1943. In addition, the problem of determining particle thickness using stereoscopic techniques, and the combination of ED with microscopy for the study of thermal modifications of kaolinite were also demonstrated. Thus, many of the capabilities of TEM for clay-mineral studies were manifest during this early period.

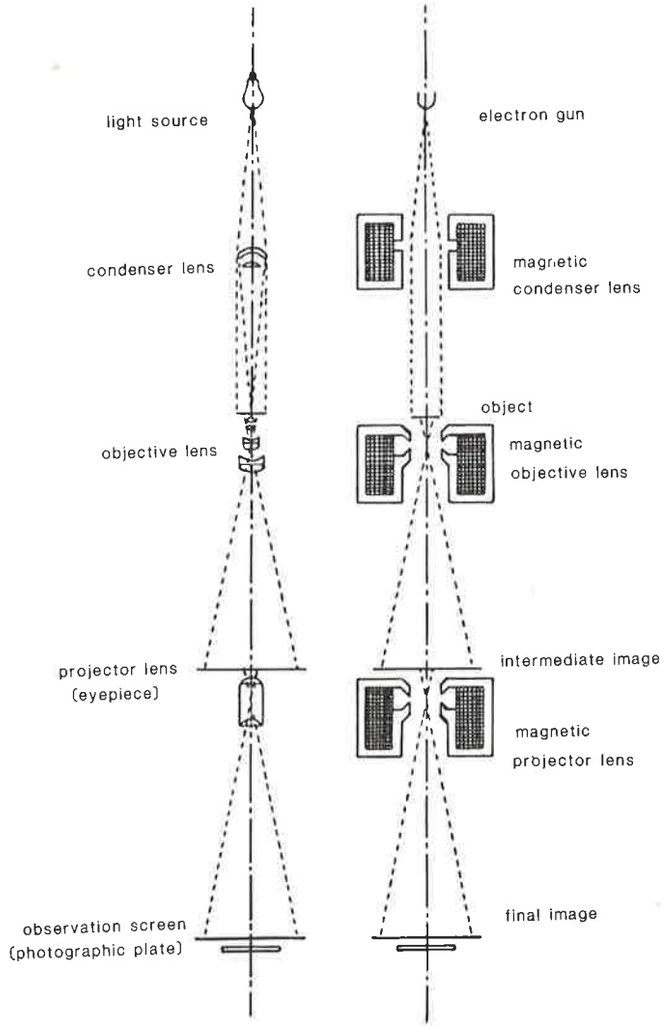

Figure 6.1 Comparison of the light and electron microscopes

Important contributions in later years included extensive ED studies of clay minerals (Zvyagin, 1967) using electron-diffraction camera and oblique texture techniques. More recent improvements in resolution have allowed examination of lattice-fringe images, which provide one-dimensional, and in certain cases, two-dimensional structure images (Yada, 1967; Iijima and Buseck, 1978), with a lattice resolution of 2 Å. A notable atlas of clay mineral micrographs was provided by Beutelspacher and van der Marel (1968). More

detailed compilations of electron-optical data of clays, including specimen preparation techniques, were provided by Gard (1971) and more recently by Smart and Tovey (1981, 1982) and Sudo *et al.* (1981).

6.2 Principles

6.2.1 *Image formation*

The goal of electron microscopy is to obtain an exact image of a specimen. In practice, however, such an absolute image is unattainable, due to the scattering between the incident radiation and the specimen. The magnitude of the scattering effect determines the limit of resolution and is directly proportional to λ, the wavelength of radiation. For visible-light microscopy, where $\lambda = 5200$–5800 Å, the theoretical maximum resolution is 0.2 μm (2000 Å). The TEM employs an electron beam which can be regarded as having $\lambda = 0.02$–0.05 Å, and can obtain images of specimens with a resolution up to 2 Å. This increase in resolution is of great value for the study of clay minerals and other microcrystalline phases.

The contrast of micrographs recorded in transmission geometry is produced by variation in the electron density in the specimen. High electron density areas of the specimen scatter and absorb more of the electron beam and thus appear dark, whereas low electron density areas appear light. For clay particles of relatively uniform composition, thicker particles appear darker than thinner ones (Figure 6.2(a)). Similarly, areas where elements of high atomic number are present are darker than those made up of elements with lower atomic number. This can be demonstrated for clay materials, when iron-

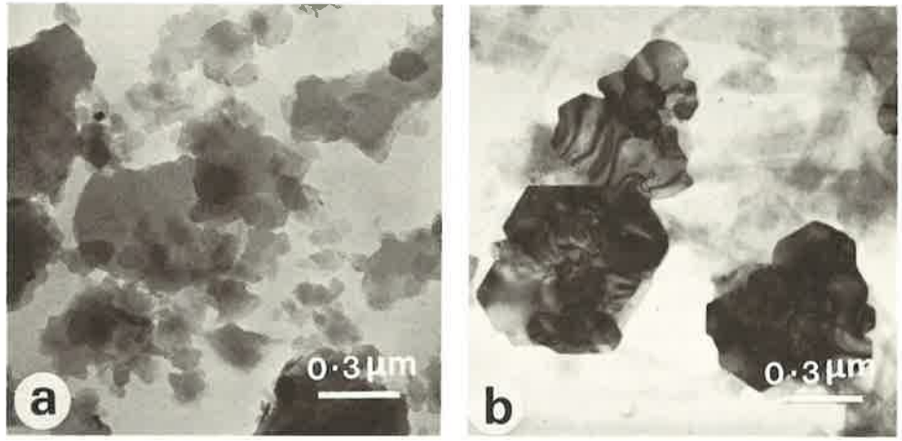

Figure 6.2 Micrographs demonstrating the effect of (a) particle thickness and (b) composition (iron oxide v. aluminosilicate) in image contrast

bearing phases, which appear darker, are present with aluminosilicates, which appear lighter (Figure 6.2(b)). Using this principle, shadow casting by evaporating metals of high atomic number, such as platinum or gold at low incident angles, has been developed to improve image contrast of thin clay particles (see section 6.4.3).

6.2.2 *Electron radiation and electromagnetic lenses*

Electrons are charged particles which have a rest mass of 9.107×10^{-28} grams. The interaction of scattered electrons, however, can be treated as a wave phenomenon, and de Broglie showed that the wavelength of the moving particles could be calculated by the following equation:

$$\lambda = \frac{h}{mv}$$

where λ = wavelength, h = Planck's constant (6.6×10^{-27}), m = mass of the particles, and v = velocity of the particles. The velocity of the electron beam in the TEM is controlled by the accelerating potential (50–400 kV). At 80 kV, the velocity exceeds half that of light, and the particles gain mass due to relativistic effects. Taking this into account, the wavelength can be calculated (Gard, 1971) from the accelerating voltage (in volts, V) from the relationship:

$$\lambda = 12.27/[V(1 + 0.978 \times 10^{-6}V)]^{1/2}$$

This relationship is shown in Figure 6.3.

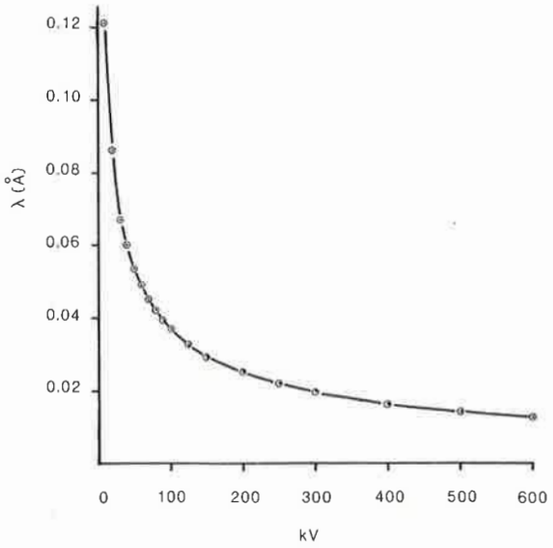

Figure 6.3 The relationship between the effective wavelength, λ, of generated electrons v. accelerating voltage (kV)

6.2.3 *Electron diffraction of small crystals*

Crystalline particles that are sufficiently thin to be transparent to electrons diffract a number of parallel electron beams, which form a primary diffraction spot pattern in the back focal plane of the objective lens. A geometric representation of this phenomenon is provided by the Bragg Law (see Chapter 2). Here the crystal is considered to consist of a number of parallel planes which repeat at regular intervals, d, and scatter the incident electron beam. At certain angles (Θ) between the electron beam and the atomic planes, the path difference between the scattered electrons is $n\lambda$, where n is an integer 1, 2, 3, etc., and λ is the wavelength of the electron beam such that:

$$n\lambda = 2d \sin \Theta$$

At these 'Bragg angles' diffraction maxima may occur, and the spacing between the planes, d, can be calculated where λ and Θ are known. The wavelength of electrons is very small, and so 2Θ does not exceed 5° over most of the diffraction pattern, and the approximation:

$$d = \lambda L/R$$

is often used, which is accurate to 0.1% for $d > 1$ Å, where L is the camera length (distance from specimen to the recording plate) and R is the distance from the diffraction maxima to the direct beam spot (000).

To determine the cell dimensions by ED it is desirable to orient the crystal so that a principal zone axis is obtained, and most instruments employ tilting stages for this purpose. For example, to obtain the a and b cell dimensions of most clay minerals, it is useful to find a [001] zone axis, the diffraction pattern of which can be indexed as hk0 (Figure 6.4). For most layer-silicate clay minerals the condition that $h + k = 2n$ applies, and maxima with indices 100, 010, 120, etc. are absent. Although it is convenient to index such a pattern as hk0, for a three-dimensional lattice, the monoclinic symmetry commonly applied to most layer silicates, requires that the spots (diffraction maxima) correspond with hk reciprocal lattice rows. To correct the a cell dimension derived from h00 ED maxima for monoclinic geometry, it should be multiplied by $\sin \beta$.

When the clay particle is oriented properly with respect to the electron beam, the symmetrically related diffraction maxima are uniform in intensity, for example, $020 \sim 0\bar{2}0$, $110 \sim \bar{1}10$, and $1\bar{1}0 \sim \bar{1}10$. The higher-order maxima are more sensitive to crystal orientation, and therefore the uniform intensity of the 060–0$\bar{6}$0, 330–$\bar{3}\bar{3}$0, and 3$\bar{3}$0–$\bar{3}$30 pairs are better indicators of proper orientation. Fortunately, layer silicates have a β angle which is sufficiently close to 90°, and most clay particles are sufficiently thin, so that particles lying on 001 require little or no tilt to yield uniform hk0 patterns. Thicker particles generally require more precise orientation, and sometimes it is necessary to slightly tilt the specimen to obtain uniform [001] zone maxima.

The relative intensities of ED maxima from thin crystals composed of

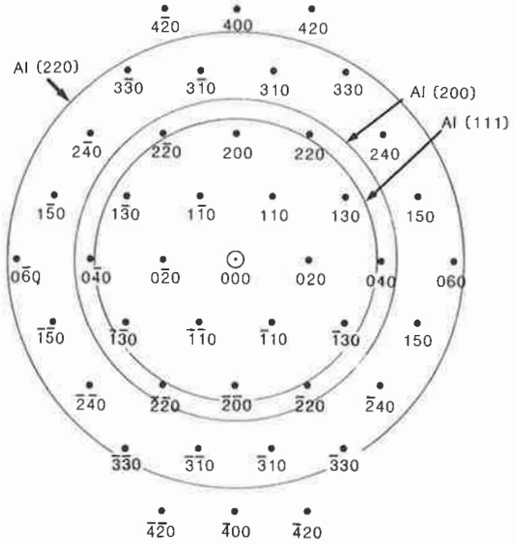

Figure 6.4 Indexing of an hk0 single-crystal spot pattern from a typical layer silicate with $b = 9.0$ Å. Also shown are diffraction rings from aluminium, commonly used as an internal standard for calculation of d-spacings

elements with moderate to low atomic number, where the intensity of the diffracted radiation is very small relative to the incident beam, can be treated as kinematic. Such kinematic intensity calculations can be used to determine the electron-density distribution of the specimen, and so provide good approximations for crystal structure analysis (Vainshtein, 1964).

Detailed discussion of this aspect is beyond the scope of this book, but in general, for thicker crystals the intensity of the diffracted radiation becomes large, and the effects of multiple diffraction (diffraction of diffracted radiation) produces complex dynamic interactions such as moiré fringes, Kikuchi line patterns (Hirsch *et al.*, 1965), and convergent beam electron-diffraction patterns (Steeds, 1979). For conventional ED studies of clay particles, the critical crystal thickness beyond which diffraction becomes dynamic has been estimated at 25–60 nm (Vainshtein, 1964), and specifically for muscovite as 36 nm—for the strongest diffraction maxima, 331—at an accelerating voltage of 80 kV (Grim and Güven, 1978). It should be noted that this critical thickness refers to crystals, not aggregates, and the electron diffraction of thick aggregates composed of thin crystals can still be treated as kinematic. Most clay crystals are thin enough to allow kinematic approximations to be used in the study of the relative intensities of single-crystal hk0 spot patterns and polycrystalline hk ring patterns.

Electrons interact with matter $\sim 10^4$ times more strongly than do X-rays, and it is therefore possible to obtain electron-diffraction patterns from

microcrystalline particles with insufficient periodicity to produce useful X-ray maxima. However, the small volume element examined by ED always raises the question of whether an observed diffraction phenomenon is representative of the bulk specimen. Further developments in ED of clays could lie in structural analysis, using statistical studies of single-crystals from a large number of observations. Important contributions have already been made in this area (Méring and Oberlin, 1971; Grim and Güven, 1978), in addition to analysis from oblique-texture polycrystalline powder patterns (Zvyagin, 1967).

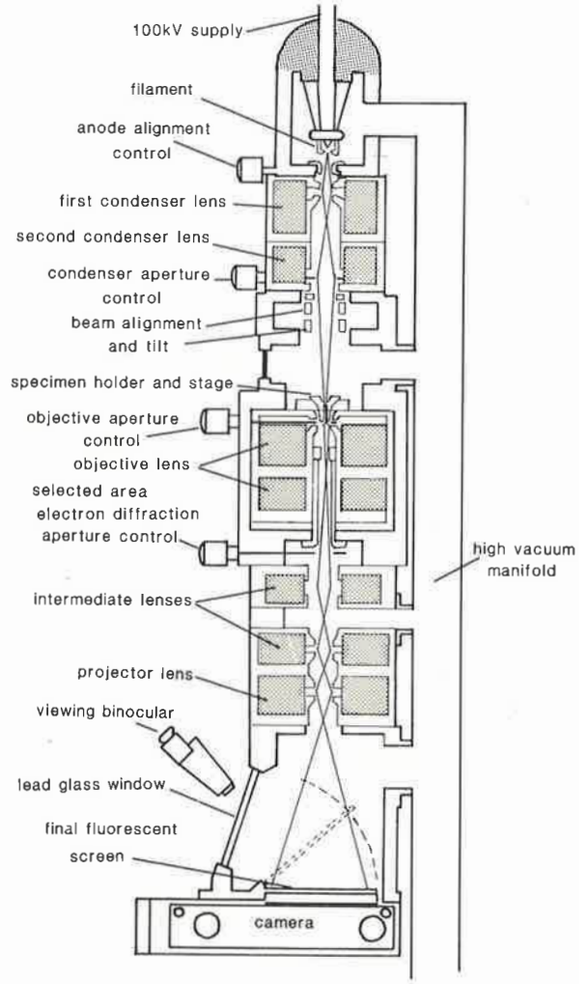

Figure 6.5 Schematic diagram of the configuration of a six-lens instrument

6.3 Instrumentation

6.3.1 *Instrument configuration*

Transmission geometry requires a linear arrangement, with the specimen lying between the electron source and observation screen. This is usually accomplished on an evacuated (10^{-4} torr) vertical column, with the electron gun at the head, followed by the first and second condenser lenses and condenser aperture, specimen chamber, objective aperture and lens(es), intermediate aperture and lens, projector lens(es), and fluorescent screen (Figure 6.5).

The instrument can be converted from imaging to diffraction mode by adjusting the intermediate lens current so that the primary electron-diffraction (ED) pattern is focused on the object plane of the projector lens and appears on the viewing screen enlarged several hundred times (Figure 6.6). The objective aperture must be withdrawn because the primary diffraction pattern is formed by electrons scattered beyond the edge of the aperture. For selected-area diffraction (SAD), see Figure 6.6(d), a diffraction aperture is placed below the position of the objective aperture, which allows diffraction from an area as small as 0.1 μm in diameter.

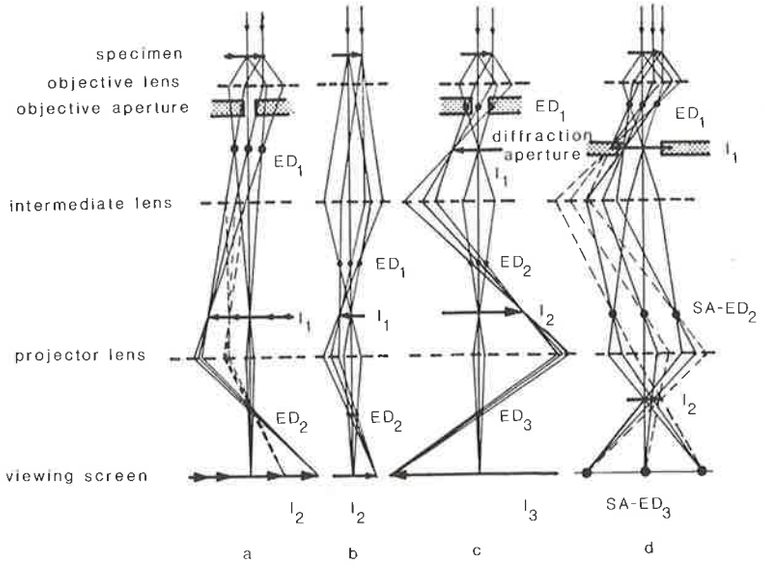

Figure 6.6 Ray diagrams for microscope with three imaging lenses: (a) Low magnification; the primary image is in the object plane of the projector, and its magnification can be reduced by the intermediate lens acting as an objective. (b) Very low magnification, with the objective lens switched off, and the intermediate lens acting as an objective. (c) High magnification; all three imaging lenses give magnified images. (d) Selected-area electron diffraction (SAD); the intermediate lens is adjusted to image the initial diffraction pattern (ED_1) in the object plane of the projector.

6.3.2 *Electron generation sources and lenses*

The electron source serves as the illumination system for the TEM imaging mode, as a monochromatic source of radiation in the diffraction mode and as a microprobe in the analytical mode. Many of these operations are performed at a variety of magnifications, and so the electron source must be versatile, and capable of high intensity. The accelerating voltages of most instruments range from 20 kV to 200 kV, and for most clay materials 100 kV is a reasonable compromise between performance and equipment costs. The source of electrons is commonly a hairpin tungsten filament.

The first condenser lens reduces the image of the source and condenses the beam, which is then focused on the specimen by the weaker second condenser lens. The area of illumination can be reduced to 1–2 μm, so that the image is bright at high magnification. The second condenser is adjusted so that the field of illumination is uniform at various magnifications, this adjustment being automatic on some instruments.

6.3.3 *Specimen chamber*

The specimen is supported on a grid, usually 3.05 mm in diameter. The specimen grid is held in a cartridge and placed onto the specimen stage in the microscope, via an access port in the instrument column. The stage can be positioned relative to the electron beam by manual or automated micromanipulators so that the entire grid can be examined. A goniometric specimen stage allows up to 60° tilt and can be used for ED studies, as well as for recording of stereomicrographs at lower angles ($\pm$ 5°). Two types of tilt goniometric stages are the double-tilt stage (usually motor-driven using foot-pedal switches) and the rotation-tilt stage, where the specimen grid can be rotated, as well as titled in one direction. The determination of the effective tilt angle which can be obtained from these two types of stages, and the methods of obtaining symmetrical zone-axis diffraction patterns, are presented in Gard (1971).

6.3.4 *Information output devices*

Traditionally, the variable-contrast electron image and electron-diffraction pattern have been observed on a fluorescent screen near the base of the instrument column. Detailed examination is made possible by using a binocular telescope (usually 10 × magnification) on a portion of the observation screen tilted into position for optimum viewing. Below the screen, most instruments have a camera which records the images and diffraction patterns on photographic film. Modern instruments may also be equipped with a scanning electron beam and detectors which produce an image on video output devices; these are designated scanning transmission electron micro-

scopes (STEM). The advantages of these systems include improved microanalytical capabilities, video recording, image intensifying of weak signals (Anderson, 1968), digital image analysis, and digital analysis of diffraction patterns (Tokiwai *et al.*, 1983). Furthermore, the video images can be more readily combined with microanalysis data.

6.4 Specimen preparation

6.4.1 *General clay preparation techniques*

As most bulk clay materials are complex mixtures containing coarse grains and organic matter, it is usually necessary to separate the fine-grained clay particles for TEM study. The $< 2\,\mu$m fraction is usually obtained using aqueous dispersion procedures: the method chosen greatly influences the material observed by TEM. Procedures should be adopted to maintain sample purity and avoid possible contaminants. The following can all contribute to sample purity: disposable pipettes and small specimen holders; ultrasonic baths for assisting dispersion and cleaning laboratory ware (ultrasonic probes may introduce fragments from titanium metal tips); microcentrifuges which can accommodate 1–2 ml volumes; a drying oven dedicated solely to microscope specimens; a dust-free laboratory environment; a readily available supply of freshly distilled water; and refrigeration for short-term storage of sample suspensions. The mildest possible procedure should be chosen in order to separate and purify the clay while avoiding the introduction of contaminants. In many cases the $< 2\,\mu$m fraction can be easily obtained from mechanically disaggregated material in aqueous suspension, which is then sedimented. Grinding, when necessary, should be done under a liquid, preferably alcohol. In some cases, carbonate material may be removed by treatment with acetic acid (25%) until the residue no longer effervesces when tested with dilute HCl. Organic material can be removed using dilute H_2O_2, and amorphous iron, aluminium oxide, and silica materials can be extracted using 0.2 M ammonium oxalate solution (Smith, 1984). Retention of highly dispersed material can be ensured by using dialysis tubing at the final stages of washing or removal of soluble components.

Clay materials are often composed of aggregates of small particles that possess a large number of unsatisfied surface charges balanced by external cations or anions. Various dispersing agents and procedures may be necessary to disperse the aggregates, the particular procedure being determined by the type of clay present. For this reason it is desirable to characterize the specimen by XRD or infrared spectroscopy, so that the appropriate dispersion technique is applied. The clay material in the $< 2\,\mu$m fraction is commonly in an aggregated state, and further dispersion is often required.

The dispersibility of a clay is determined in part by the type of ion on its surface. Na^+ and Li^+ are cations with high dispersing properties. Aggregated clays can be dispersed by first placing the material in a 1 M chloride salt solution, followed by agitation, centrifugation at high speed, decanting, and suspension in fresh salt solution. The procedure is repeated, so that the clay is washed three times, once overnight. After final centrifugation, the salt solution is decanted, the clay is suspended in distilled water, and the remaining excess ions are removed by dialysis against de-ionized or distilled water until free of chloride ion. The clay in suspension will now be highly dispersed, and can be further size-fractionated by centrifugation. The optimum size-fraction varies from sample to sample. The following fractions are suggested: $< 0.5\,\mu$m for well-crystallized illites and chlorites, $< 0.2\,\mu$m for poorly crystallized illites and interstratified clays with less than 40% smectite layers, and $< 0.1\,\mu$m for smectites and interstratified clays with $> 40\%$ smectite layers. The suspension should be characterized by XRD of its sedimented aggregate, even when the suspension appears to be water-clear. Vermiculites and vermiculite interstratifications are difficult to study by TEM because they are often composed of large particles inherited from parent mica crystals. These clays can, however, be treated with large organic cations such as the *n*-butylammonium ion, so that they exfoliate in aqueous systems (Walker, 1967), so producing thin particles which can be more readily investigated. Kaolinitic clays (dickite, kaolinite and halloysite) often disperse well with small amounts of sodium pyrophosphate (1 mg/g clay) or sodium hexametaphosphate (1 ml of 0.1 M Calgon: 100 ml of water: 1–5 g of clay). Small amounts may be added to most clay suspensions to inhibit the reaggregation of clay particles after dispersion. The $< 1\,\mu$m fraction is recommended for well-crystallized kaolinite. Unlike most clays, imogolite disperses in acid conditions. Farmer *et al.* (1980) recommended a pH of 3.5 (0.001 M HCl) with ultrasonic treatment. For TEM studies the $< 0.5\,\mu$m fraction is recommended.

6.4.2 *Specimen supports*

A good general-purpose specimen support for clay materials is a thin 200-mesh copper grid, with a centre disc indication and a rectangular pattern made of different width axis bars to aid in orientation and location.

A carbon support film rests upon the grid. This film is made by evaporating a 2 nm carbon layer onto a freshly cleaved sheet of mica, using a vacuum-coating apparatus equipped with a thickness gauge. The carbon-coated mica sheet is then carefully immersed in distilled water, so that the carbon film separates and floats on the water surface (Figure 6.7). The copper grids (shiny side up) are then immersed in the water and placed on a wire gauze, which is then carefully positioned under the floating carbon film, and raised so that the film uniformly covers the grids. Following this treatment, the grids are placed on a clean piece of filter paper and allowed to dry. The grid is then placed shiny side down and attached to a support arm, and a small drop of the clay suspension is applied to it. The grid is then placed in a drying oven at 50°C.

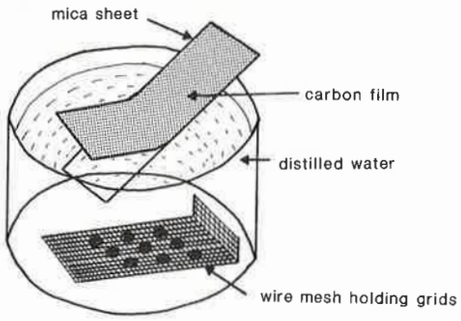

Figure 6.7 Flotation of carbon film from the mica sheet onto water with support grids on wire mesh in the bottom of the dish

Frequently, the concentration of clay particles is too high, and the film is cluttered with overlapping particles. In this case, the clay suspension should be diluted, further dispersed in an ultrasonic bath, and re-examined until an optimum dispersion is obtained. As a general rule it is necessary to dilute the clay suspension until only a faint scattering of light can be observed. For fine clay fractions, i.e. $< 0.2\ \mu$m esd (equivalent spherical diameter), the suspension is diluted until water-clear.

6.4.3 *Shadow casting*

This is a useful technique for improving contrast, and for the quantitative determination of thickness. Very thin clay particles, such as smectites and interstratified clays, may be difficult to resolve. In such a case, a drop of the diluted clay suspension is spread over a sheet of freshly cleaved mica and allowed to dry. The mica sheet is then carefully attached to a shadowing stage with a projection of known height (such as a 2–3 nm screw head) and placed in a vacuum-coating apparatus equipped with a thickness gauge. The stage is set so that it is titled to $\sim 10°$ with respect to the shadowing source, and Pt metal is evaporated onto the area, until the gauge registers 6 nm. The stage is then placed perpendicular to the shadowing direction and coated uniformly with 2 nm of carbon. Once removed, the projection on the stage should cast a visible shadow 10–15 mm in length, which can be measured ($\pm$ 0.05 mm) to determine accurately the shadowing angle, using the relationship:

$$\tan a = h/l,$$

where a is the shadowing angle, h is the height of the projection and l is the shadow length. The mica sheet is then carefully immersed in distilled water so that the carbon film with the Pt-shadowed clay particles floats and is picked up on the copper grids (Figure 6.7). TEM examination should show that the edges

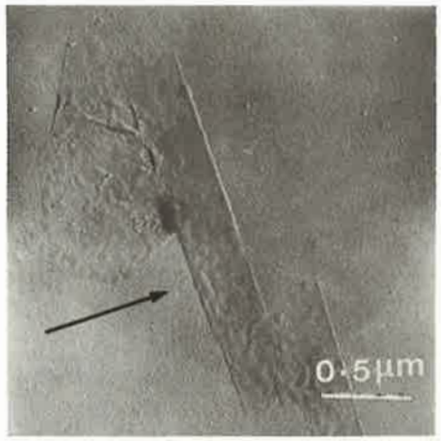

Figure 6.8 Shadow-cast preparation of beidellite; arrow indicates shadowing direction

of the particles lying towards the Pt source have accumulated fine-grained metal and appear dark, whereas the edges of the particles lying away from the platinum source have cast a shadow where no Pt grains are present and therefore appear light. The longer the shadow, the greater the thickness of the particle. In this way, the contrast of the particle edges is enhanced (Figure 6.8). The technique also allows determination of particle thickness. By measuring the length of the shadow parallel to the shadowing direction, the particle thickness (T) is given by:

$$T = (l \times \tan a)/m$$

where l is the shadow length, a is the shadowing angle, and m is the magnification of the micrograph. When the shadow length is not measured exactly perpendicular to the shadowing direction, the value T is divided by the cosine of the angle of deviation. This technique is accurate to $\pm$ 0.4 nm, and can measure particles as thin as 1.0 nm. More details on this technique and its uses are given in section 6.5.3.

6.4.4 *Replicas*

It is possible to study the orientations and configurations of clay particles from the surface features of a bulk sample, using replica techniques. A variety of techniques exist (Comer, 1971). The Pt/C-shadowed replica method is useful for clays. This technique is analogous to the procedure described in the previous section, except that, after coating, the specimen is placed in 48% hydrofluoric acid, so that it dissolves to leave the Pt/C replica. The replica film is then water washed, placed upon a copper grid and examined (Figure 6.9).

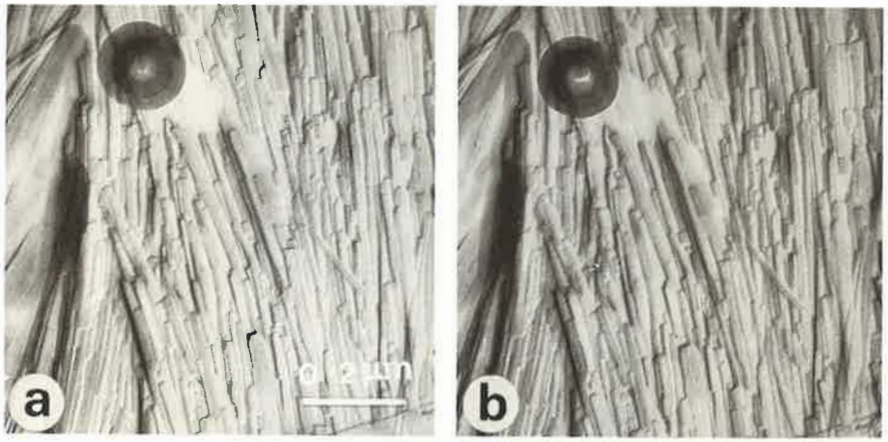

Figure 6.9 (a) and (b) stereopair of a replica of a fracture surface of sepiolite

Surface features up to 2.5 nm in relief are observable with this technique. Diffraction or microanalysis studies are not possible because of the acid dissolution of the specimen.

6.4.5 *Microtome sections*

Microtome sections are useful because they enable the orientation of clay particles with their *c*-axes perpendicular to the electron beam. This edge-on orientation is necessary for the study of local lattice images and 001 diffraction (section 6.6.1). Drops of clay suspensions can be dried on a cured epoxy surface, and the resulting sedimented aggregate can be 'sandwiched' by the addition of more epoxy (Spurr, 1969). Alternatively, fine-grained clay, such as that obtained from freeze-dried suspensions, can be gently mixed into the liquid epoxy and cured. Several varieties of epoxy and impregnation techniques are available, and some that form stable complexes with expansible clays (Yoshida, 1973) have been developed. The cured epoxy block is trimmed and mounted on an ultramicrotome (Reid, 1975). Sections less than 50 nm thick are then cut, preferably using a diamond knife, floated on distilled water, and picked up on copper support grids. Sections should be coated with 2 nm of carbon prior to TEM examination, to enhance their stability in the electron beam.

6.4.6 *Ion-beam thinning*

This is an alternative method of preparing specimens for lattice-fringe image study (Paulus *et al.*, 1975; Bresson, 1981). It is generally performed on small

samples of bulk material impregnated with epoxy, which are ground to $\sim 30\,\mu$m in thickness. The section is inspected using an optical microscope, and then mounted in a vacuum ion-beam milling apparatus, where an intense ion beam perforates the section. It is then mounted on a copper grid and examined by TEM. Images are observed at the thin edges of the section, near perforations. Ion-beam thinning is recommended for study of bulk specimens which contain coarse materials (such as quartz) that would otherwise damage the knife of a microtome. With heterogeneous specimens, however, it may not be clear whether the lattice images obtained originate from fine-grained clay materials, or from coarse-grained phyllosilicates.

6.5 Analytical procedures for clay materials

6.5.1 *Operating conditions*

The observation of clay materials can be adequately carried out at operating voltages of 100 kV. Higher voltages, however, offer greater resolution, and in general, slower rates of beam damage to sensitive materials. Furthermore, the sample penetration depth can be improved by a factor of ~ 1.7 when the operating voltage is increased from 100 kV to 200 kV.

Although most clay materials are relatively stable in the electron beam, radiation damage of the specimen is sometimes observed under the operating conditions for TEM. In some diffraction patterns and lattice-fringe images the effects can be seen as a gradual loss of detail, and in other instances, there is damage in the form of physical distortion and change in contrast. These effects are most severe at high magnification, and, therefore, appropriate operating procedures can be adopted to minimize exposure to high beam intensities until immediately before micrograph recording (Agar, 1978). These procedures include general observation at low magnification, prefocusing on a region of the field not including the area of interest, and avoiding unnecessary exposure to the beam.

6.5.2 *Specimen assessment*

When examining specimens that have been subjected to dispersion and size-fractionation procedures, the distinction between aggregates and particles should be borne in mind. (Yariv and Cross, 1979, refer to aggregates as secondary particles). Primary particles are considered to be free and distinct, whereas aggregates are complex arrangements of primary particles. Aggregates are commonly observed at low magnifications ($\times$ 10 K–20 K), whereas primary particles are commonly observed at higher magnifications. Sometimes primary particles are large and easy to resolve, as in kaolinite (Figure 6.14), but in smectites, the primary particles are very small and the distinction is more obscure. Shadow-casting techniques can be employed to

improve contrast of small primary particles (section 6.4). Sometimes it may not be clear whether the observed aggregates derive from the bulk specimen, or if they have been formed in suspension or after drying.

Size-fractionated material can be very different from the bulk clay, particularly when the samples are composed of mixtures of clay minerals, and characterization of the various fractions by an independent method such as XRD is advised to guard against any bias introduced during sample preparation. Other minerals may also be present in the specimen; often, phases not detected by conventional methods are observed by TEM, including, for example, goethite and hematite in sediments, and lepidocrocite, goethite, gibbsite and boehmite in soils (Mackenzie *et al.*, 1971). Introduction of contaminants and spurious features by sample preparation methods must also be assessed. The presence of trace amounts of salt, resulting from incomplete removal of excess ions, is indicated by graininess on the specimen support film, and by the characteristic electron-diffraction pattern of the halides. Where concentration of the suspension has been achieved by evaporation, the precipitation of sparingly soluble microcrystalline phases such as baryte may occur. Concentration of fine-grained material by ultracentrifugation is preferable, followed by resuspension of the pellet in a smaller volume of distilled water.

6.5.3 *Data acquisition*

Examination of clays should proceed from low (10 K) to high magnification (100 K), encompassing as large an area of the specimen as possible, so as to obtain a representative assessment of the overall character of the material. After obtaining this overall impression, electron micrographs and electron-diffraction patterns should be acquired, to characterize the clay. The image should be focused using the telescope and tilting screen, to the optimum, slightly underfocused condition.

The morphological characteristics of clay particles and aggregates are often described in the following terms (examples are given in brackets).

Particles:

plates:	most clay particles can be regarded as plates with large lateral dimensions relative to thickness
lath:	a flat, elongated particle, (e.g. illite, hectorite, nontronite); curled and folded thin particles can also appear to be lath-like (e.g. beidellite)
euhedral:	particles showing straight edges, usually psuedo-hexagonal, indicative of crystal habit (e.g. kaolinite, illite, rectorite)
subhedral:	particles showing irregular edges (smectite, chlorite)
equant:	particles whose areal dimensions are approximately equal (kaolinite)
subequant:	particles whose lateral dimensions are unequal, but to a lesser degree than laths (illite, smectite)

fibres:	particles which exhibit extreme elongation, greater than that of laths (palygorskite, sepiolite, chrysotile)
tubes:	particles which have hollow cylindrical forms, (halloysite, imogolite, chrysotile)

These terms can be combined in certain ways, such as tubular fibres (chrysotile), and euhedral plates, (kaolinite). Particle morphology is not necessarily indicative of the mineral type, and some clay minerals, such as illite and rectorite, display a variety of forms, from euhedral laths to equant plates. On the other hand, some forms are completely characteristic, as in the case of imogolite.

Aggregates:

lamellar:	tabular, platy, flat material
foliated:	folded or crumpled material (smectites)
vermicular:	elongated worm-like material (kaolinite)
fibrous:	radiating or oriented arrangements of elongated particles
mosaic:	component particles appear to have crystallographic relationships
irregular:	composed of random arrangements of particles
polyphase:	composed of more than one mineral.

As is the case for particle terminology, combined terms can be used, such as mosaic-fibrous (exhibited by some illites) and foliated-lamellar (smectites).

New perspectives on clay morphology can be gained by studying stereoscopic images from micrograph pairs taken at different tilt orientations (using the goniometric specimen stage, Figure 6.9). With a tilt angle of 10°, (+ 5° for one micrograph, and − 5° for the other, across the tilt axis) resolution of features 200–500 nm in size can be achieved at magnifications of × 50 K to × 100 K. The micrograph pairs must be oriented correctly (N–S), with respect to the stereoscope viewer (E–W). Where this task is complicated by image rotation, a method for calculating the effective tilt-axis direction with respect to the micrographs can be used (Gard, 1971). Micrographs can usually be oriented and mounted properly by trial and error.

Statistical particle-size distribution analysis provides valuable information concerning the nature of clay material (Nadeau *et al.*, 1984b, 1985; Nadeau, 1985). These studies were conducted on Pt/C-shadowed specimens, usually from well-dispersed, size-fractionated suspensions. Conley (1966) and Bates (1971) reported measurements of particle length (L), width (W), and thickness (T), mean particle diameter, $(L \times W)^{1/2}$, and shape factor O $(T/(L \times W)^{1/2})$ for kaolinite. In such studies, for accurate thickness determination it is important that representative, flat-lying particles are measured, with no obstructions in the shadow area. Satisfactory preliminary results can be obtained from 10–30 particle measurements, and for detailed studies, 100–200 particles. The use of a digitizing tablet for micrograph analysis also allows the determination of particle area (A), and perimeter (P) which, when combined with the thickness

(T) of planar particles, allows the calculation of volume ($V = T \times A$), basal surface area ($A \times 2$), and edge surface area ($T \times P$).

If the particle density is assumed (usually 2.6 g/cm^2) then the particle mass and surface area in m^2/g can also be determined. Nadeau (1985) showed that a useful approximation of surface area in m^2/g from the particle thickness is given by the expression:

$$S = 800/Tm$$

where S is the surface area, and Tm is the mean particle thickness in nm.* The particle surface area and mass data can be combined with independent cation-exchange capacity (CEC) data to determine the average surface charge density on the clay surface. For example, a smectite sample with a CEC of 103 meq/100 g, has particles with a mean surface area of 11.04×10^4nm^2, mass of 167×10^{-18}g, and has 10.4×10^4 sites/particle, with a charge density of 1.06 nm^2/site.

Microchemical analysis of clay particles allows identification of different particle types, as well as the study of variation in clay crystal chemistry. For discrimination purposes, the ratio of the major elements is often used, such as Al/Si for kaolinite, K/Si for illite, or Mg/Si for chlorite. The analytical mode can be used for either individual particles, or for area scans which include a large number of particles. In specimens composed of very small particles, EDS systems may only provide useful information in the latter mode. Some problems with microanalysis of clays are their decomposition in the electron beam and the difficulties in obtaining reproducible determination of volatile elements such as potassium.

6.6 Electron diffraction of clay particles and aggregates

6.6.1 *General features of clay materials*

Platy clay particles and irregular lamellar aggregates commonly yield single-crystal spot patterns and polycrystalline ring patterns respectively. The single crystal pattern shows a pseudohexagonal symmetry, and can be indexed as hk0 (Figure 6.4) corresponding with an 001 section. Such patterns are observed from free and individual particles when examined by selected-area diffraction (SAD), but when a large area of the specimen is examined, many individual particles diffract and a polycrystalline ring pattern is observed. The pattern results from the hk0 maxima of randomly distributed individual particles. Similar patterns are produced by SAD of irregular lamellar

*This approximation is valid for clay materials, whose total surface area consists predominantly of basal surface area. For clays whose basal surface area accounts for only ~ 65–85% of the total surface area, such as kaolinites, the value S can be multiplied by a factor to account for the significant amount of edge surface area, which in the case of Tm = 50 nm, would be 1.24.

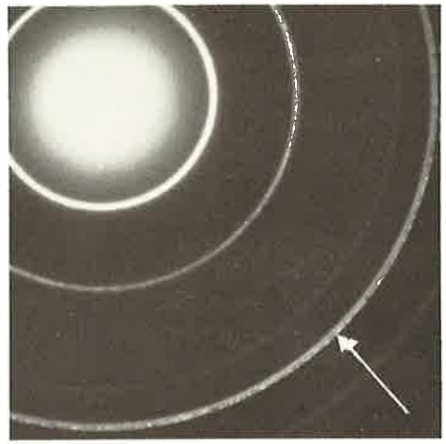

Figure 6.10 Part of a polycrystalline ring pattern with double 06 rings (arrowed) from the presence of both dioctahedral (outer ring) and trioctahedral components in the specimen

aggregates, in which the component particles are lying with their *c* axes approximately parallel to the beam but with no preferred orientation in the *ab* plane. Such patterns are often described as turbostratic. Polycrystalline patterns can be further designated as monomineralic and polymineralic, the latter consisting of sets of reflections from two or more phases. For example, the presence of both dioctahedral and trioctahedral clays can be determined by examination of the 06, 33 ring, which would have two intensity maxima (Figure 6.10).

In general, platy clay particles give very similar hk0 spot patterns, thus excluding the use of ED as a primary means of identification, this being a consequence of their similarities in structure. However, some clays, such as antigorite, tubular halloysite, sepiolite and palygorskite have characteristic diffraction features which allow unequivocal identification.

6.6.2 *Determination of d_{hkl}*

When d_{hkl} is determined using the formula $d = \lambda L/R$, (section 6.2.3), it is necessary to record the objective lens current (± 0.1 V) at the time when the diffraction patterns are recorded. In this way, a calibration curve of lens current against λL is obtained. Alternatively, an internal standard can be applied to the specimen, usually in the form of an evaporated metal such as Al or Au (Table 6.1). Using Al as an internal standard, enables determination of *d* up to 0.2% accuracy (Brindley and De Kimpe, 1961). The distance $2r_x$ between corresponding spots is measured across the direct beam spot from the negative, and the diameter $2r_s$ of the hkl ring from the standard is measured in

Table 6.1 Spacing of some internal standards for diffraction studies.

Element	d	I	hkl
Al	2.338	100	111
	2.024	47	200
	1.431	22	220
	1.221	24	311
Au	2.355	100	111
	2.039	52	200
	1.442	32	220
	1.230	36	311

a similar manner. The calculation is:

$$d_x = (2r_s)(d_{hkl})/2r_x.$$

6.6.3 *Application of* hk0 *diffraction*

When a free and individual clay-mineral particle yields a single-crystal diffraction pattern, it is referred to as a fundamental particle. The crystallographic orientation of the particle can be established, and for euhedral particles the crystal forms can be identified. In the case of subequant, lath- and fibre-shaped particles, the direction of elongation can be established. Thin lath-like 1 M illite particles are commonly *a*-axis elongated, this being established by the strong (020) spots (Figure 6.11(a)). Conversely, diffraction patterns from large equant particles of $2\,M_1$ muscovites, show weak 020 spots (Figure 6.11(b)). The relative intensities of the hk0 spots are of particular interest in dioctahedral clays, because they are sensitive to the octahedral sites occupied. However, these considerations are beyond the scope of this book, and the interested reader should refer to papers by Méring and Oberlin (1971) and Grim and Güven (1978) for further details.

6.6.4 *Dark-field imaging of clay particles*

The diffraction maxima of the clay crystals can be used to create an image of the particle(s) from which the maxima originated. This is accomplished by deflecting the main beam, so allowing only the diffraction maxima to pass through the objective aperture. In this mode the background and amorphous material appear dark, and the crystalline material which contributes to the diffraction maxima appears light. This technique helps to resolve crystalline particles when they are associated with amorphous material, and also improves the contrast of very small crystalline particles.

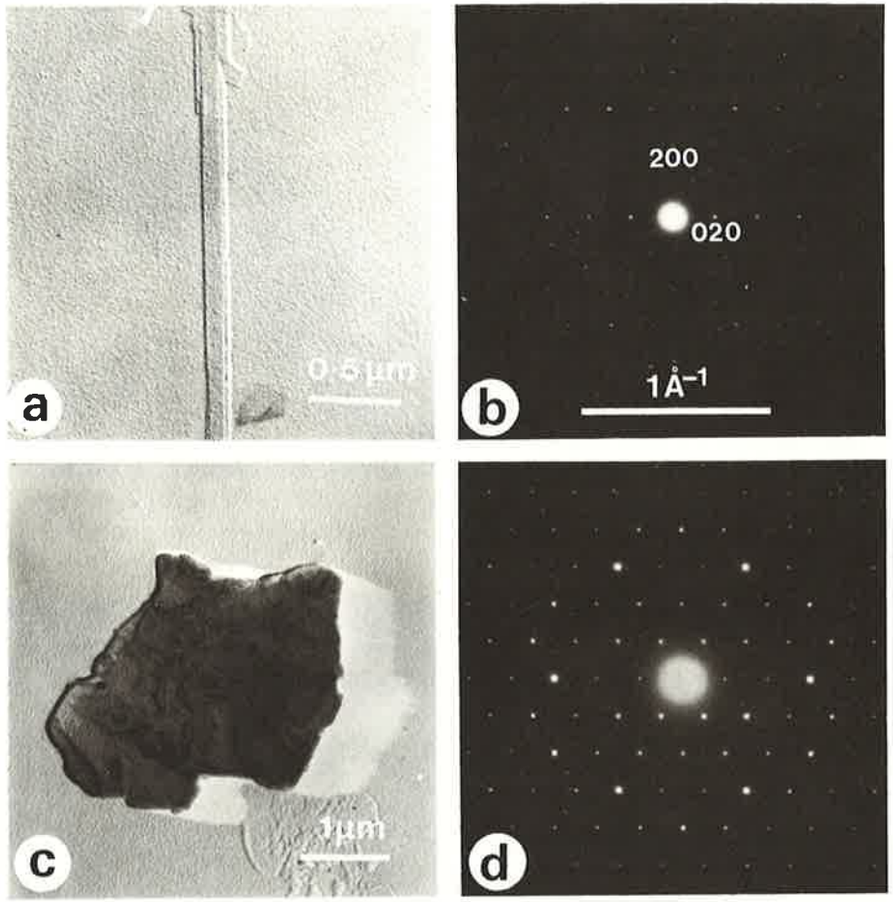

Figure 6.11 Pt/C-shadowed preparations of (a) 1M illite lath, and (c) equant $2M_1$ muscovite flake; (b) and (d) diffraction patterns from (a) and (c), respectively; diffuse rings are from Pt. The scale shown on (b) is the same for all subsequent diffraction patterns

6.6.5 *001 diffraction and lattice-fringe images*

Examination of 001 diffraction maxima requires that the *c*-axis of the clay particles should be perpendicular to the electron beam. Usually, this can only be obtained from microtome or ion-beam-thinned sections of epoxy-impregnated specimens, but sometimes particles which have curled up, or have twisted on-edge (Figure 6.12(a)), allow lattice-fringe images to be acquired in conventional preparations on a support film (Figure 6.12(b)). In clays, most lattice fringes are one-dimensional, in that only the c^* reciprocal lattice direction is normal to the electron beam. Crystals with three-dimensional

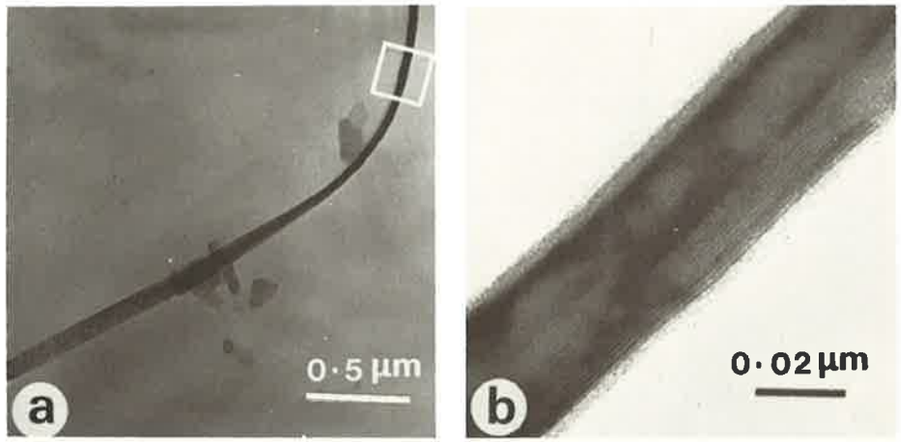

Figure 6.12 (a) Long thin illite lath which has twisted on-edge towards the top right-hand edge of the micrograph. (b) Lattice-fringe image from tilted portion of the lath with the *c*-axis perpendicular to the electron beam

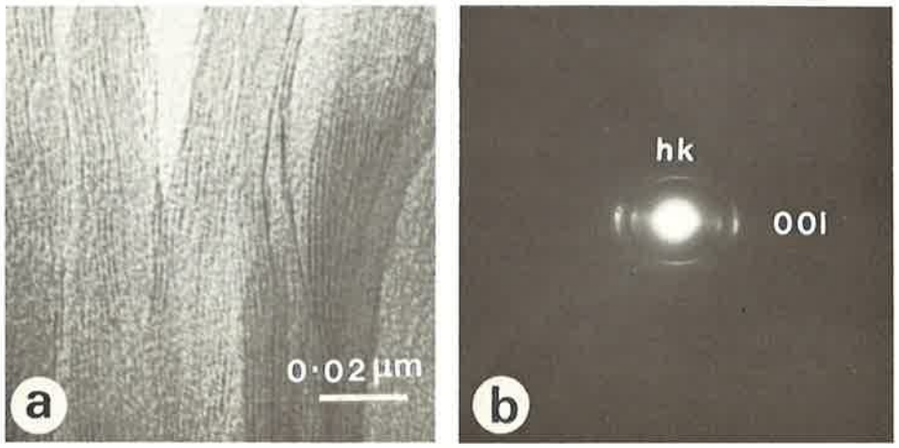

Figure 6.13 (a) Lattice-image of ultramicrotome section of montmorillonite embedded in resin. (b) Diffraction pattern showing 00l arcs and hk diffraction bands

periodicity can, however, be tilted such that a [hk0] zone axis, preferably [010] or [100], is obtained, and impressive two-dimensional lattice-fringe structure images have been obtained from large phyllosilicate crystals. Highly disordered clays, such as turbostratic smectites, have no three-dimensional periodicity and only yield one-dimensional lattice-fringe images (Figure 6.13(a)). Tilting of the specimen in the *ab* plane produces little, if any, change in the diffraction character. Instead of single-crystal spot patterns, 001

arcs and hk diffraction bands are obtained (Figure 6.13(b)). The arcs reflect the spacing between the adjacent silicate layers, and the bands represent the distribution of hk maxima from the individual layers, which are randomly arranged with respect to the *ab* plane. Lattice images may be obtained from specimens composed of aggregates of thin particles consisting of a small number of layers (3–10). A complex pattern results from a number of small single-crystals contributing to the 001 diffraction, but with no crystallographic continuity across the particle interfaces. Discrimination between particle interfaces and 'stacking faults' is difficult, and the microscopist must be aware that either can be present in the lattice-fringe images of clay materials.

6.7 Micrographs and electron-diffraction patterns of common clay minerals

The morphology of the clay minerals, as observed under TEM, has been illustrated at length in the atlases of Beutelspacher and van der Marel (1968) and Sudo *et al.* (1981). Structural information, as adduced from electron-diffraction patterns has been just as extensively discussed by contributors to the Electron Optical Monograph on Clay Minerals published by the Mineralogical Society (Gard, 1971). An illustrated overview is attempted here of the diagnostic TEM features of the main minerals occurring in clay materials. The discussion is anything but exhaustive and the reader should refer to the above publications for further details.

6.7.1 *Kaolinite minerals*

Well-crystallized kaolinite is generally unmistakeable under the TEM, and consists of relatively large, well-defined, hexagonal-shaped particles, bounded by prism and pinacoid faces (Figure 6.14(a)). The size of the particles varies widely, but often falls in the 0.5–2.0 μm range. The thickness of the kaolinite hexagonal plates usually exceeds 0.05 μm, and on average, the ratio of plate diameter to thickness (aspect ratio) is 6:1. Well-crystallized kaolinite always yields a well-defined, hexagonal, single-spot SAD pattern (Figure 6.14(b)).

Poorly ordered kaolinite is generally composed of subequant, platy particles with no particular well-developed form (Figure 6.14(c)). These particles tend to be thinner than those of well-crystallized kaolinite and yield somewhat poorer ED patterns (Figure 6.14(d)). Poorly crystallized kaolinite would be difficult to distinguish from other platy clay minerals, such as mica or chlorite, on the basis of TEM observations alone. There is no absolute correspondence between structural order and morphological perfection in kaolinites, and examples are known of poorly ordered, euhedral kaolinite and highly ordered anhedral kaolinite (Robertson *et al.*, 1954).

Dickite usually occurs as large, exceptionally well-formed, hexagonal

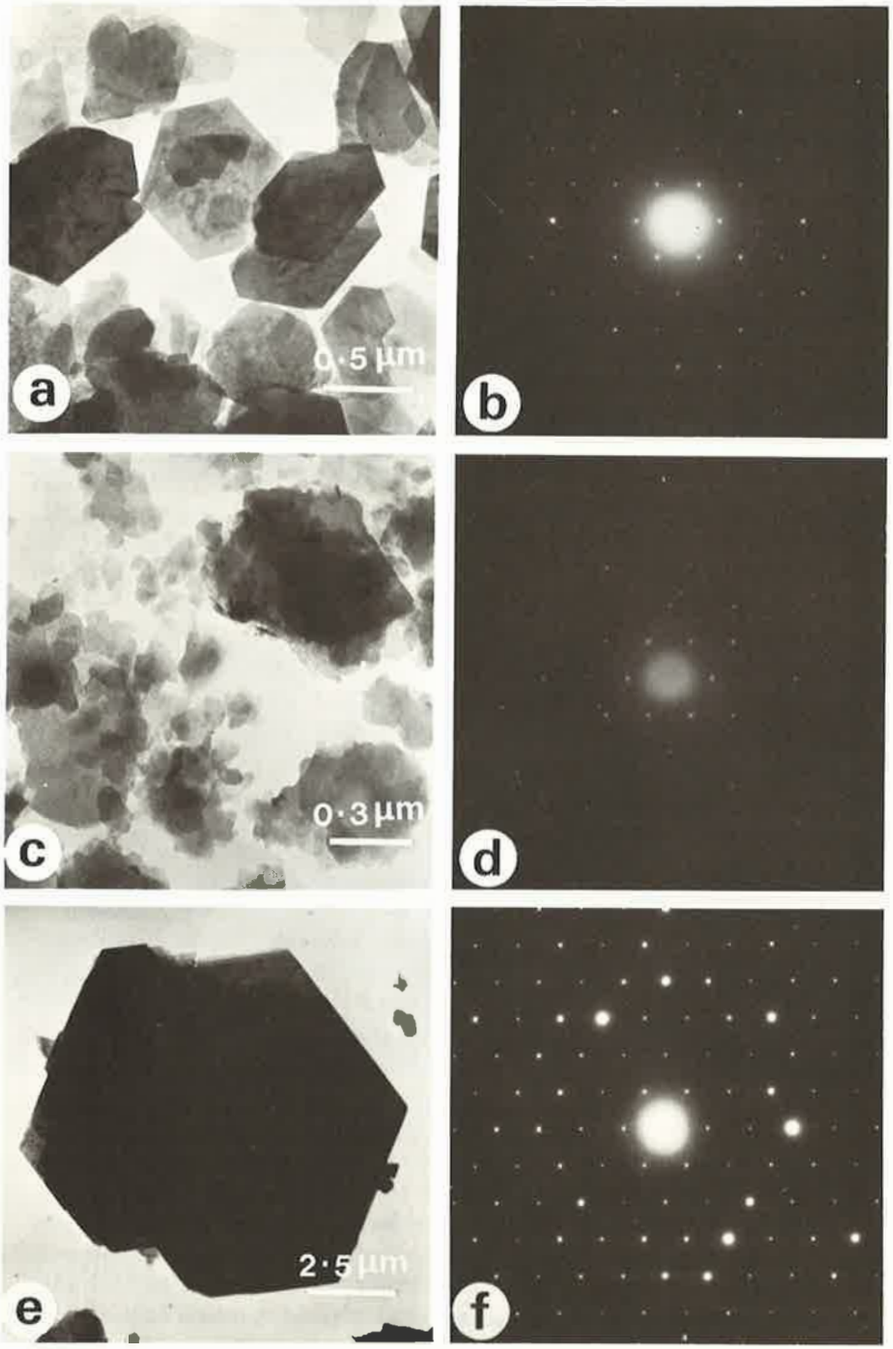

Figure 6.14 Micrographs and electron-diffraction patterns of well-crystallized kaolinite (a), (b), poorly ordered kaolinite (c), (d), and dickite (e), (f). SAD spot pattern (b) also shows rings from aluminium (Al) as on internal standard

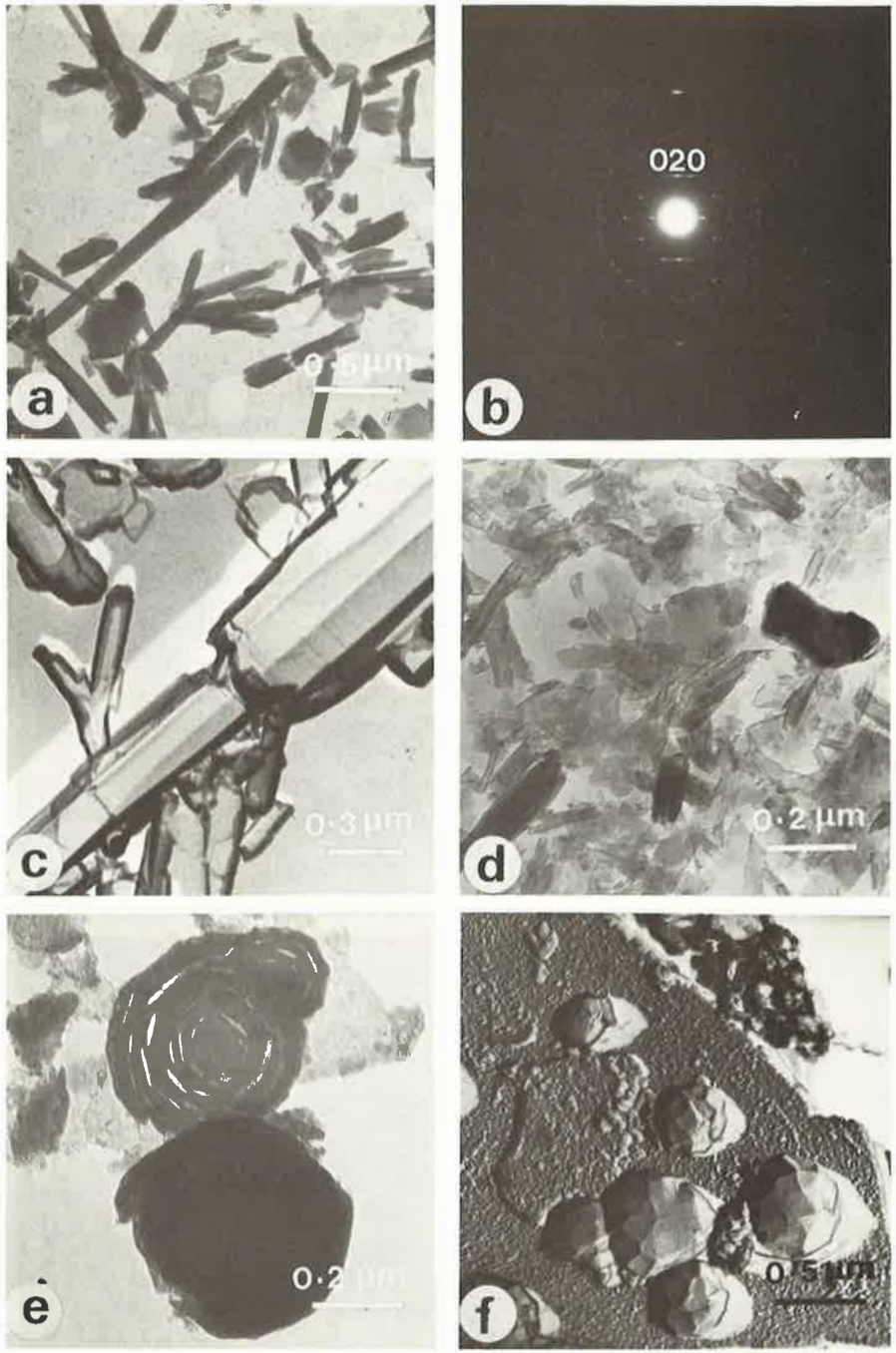

Figure 6.15 (a) Tubular halloysite: diffraction pattern (b) shows streaking along rows due to curvature of lattice in a tubular formation. Spacing between rows indicates *b*-axis elongation. Rings are from Al. (c) Replica of a well-crystallized form of tubular halloysite. (d) Halloysite with poorly developed tubular morphology. (e) Replica of spheroidal halloysite showing well-developed crystal faces. (f) Thick and thin spheroids, the latter showing spiral structure

crystals (Figure 6.14(e)), showing the prism and pinacoid faces recognized in kaolinite, and sometimes even pyramids and domes. Particles up to 0.5 mm in diameter have been found, enabling optical and single-crystal X-ray studies to be made. Most commonly, dickite occurs in the 2–50 μm fraction and should certainly be suspected if large 'kaolinite-like' particles occur in non-clay fractions. As might be anticipated, dickite yields exceptionally clear, single-crystal-type, hexagonal ED patterns (Figure 6.14(f)).

Halloysite exhibits considerable morphological variability; in its commonest form, it consists of fine, tubular or lath-like particles (Figure 6.15(a)). Replica studies of halloysite sometimes reveal the development of crystallographic faces parallel to the tube axes (Figure 6.15(c)). In some soils, however, tubular morphology is extremely poorly developed, and may amount to little more than incipient curling of the long edges of lath-like particles (Figure 6.15(d)). Halloysites separated from volcanic soils may show a quite different morphology, and may occur as spheroids (Figure 6.15(f)), sometimes revealing an unusual spiral structure (Figure 6.15(e)). In general, the morphology of halloysite is sufficiently distinct from the other kaolinite minerals for TEM observations to be regarded as quite diagnostic.

6.7.2 *Serpentine minerals*

The most common varieties of serpentine minerals can be readily recognized under the TEM.

Chrysotile is unmistakable because of its finely fibrous form, the fibres themselves giving an impression of flexibility, as they are often curved or bent (Figure 6.16(a)). Ultrastructural studies show that chrysotile has a tubular morphology, consisting of spirally rolled layers, the fibres themselves often being composed of bundles of smaller fibrils. Typically, chrysotile fibres yield an electron-diffraction pattern consisting of streaked reflections arranged in layer lines. Indexing and measurement of the pattern shows that fibres are usually elongated along the *a*-axis (Figure 6.16(b)).

Antigorite is commonly made up of platy particles with distinct rectangular outlines (Figure 6.16(c)), or of short, stiff fibres. Such a morphology is not entirely diagnostic, but the ED pattern (which is relatively easily obtained) is quite specific. This is because the mineral has a corrugated sheet structure, which leads to a hexagonal pattern characterized by distinct clusters of subsidiary spots around the main reflections (Figure 6.16(d)).

Lizardite is composed of platy particles of indeterminate shape but with strong outlines (Figure 6.16(e)). A typical single-crystal type, hexagonal ED pattern is yielded by such plates (Figure 6.16(f)), there being no indication of the subsidiary reflections found with antigorite.

6.7.3 *Chlorite and illite*

These minerals are considered jointly, because in many clay materials it would be difficult to differentiate them on the basis of TEM observations alone.

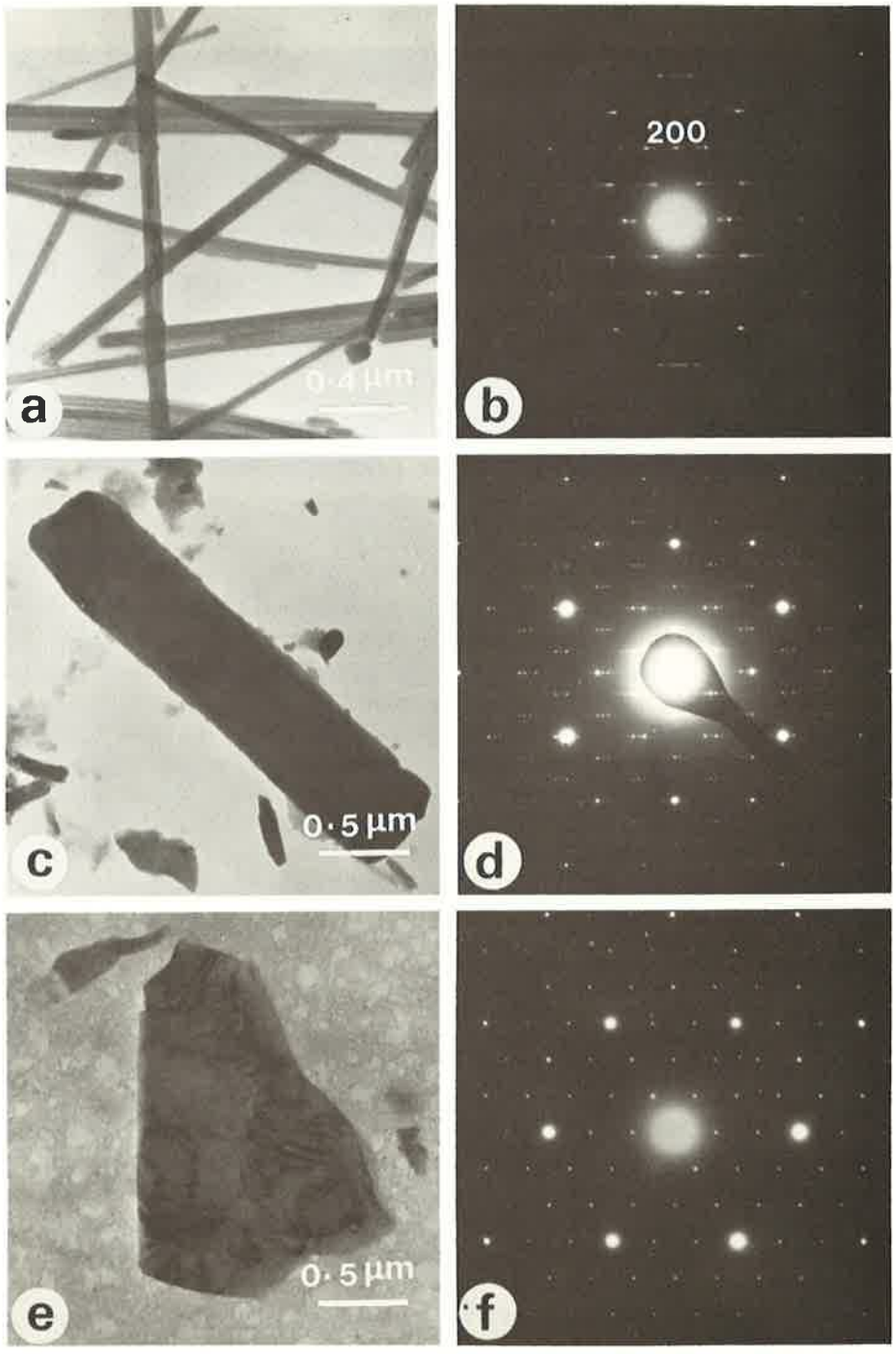

Figure 6.16 (a) Chrysotile, (b) diffraction from chrysotile indicates *a*-axis elongation. Note the spacing between layer lines compared with the halloysite pattern (Figure 6.15(b)) can be diagnostic. (c) Antigorite with characteristic diffraction pattern (d). (e) and (f) show lizardite

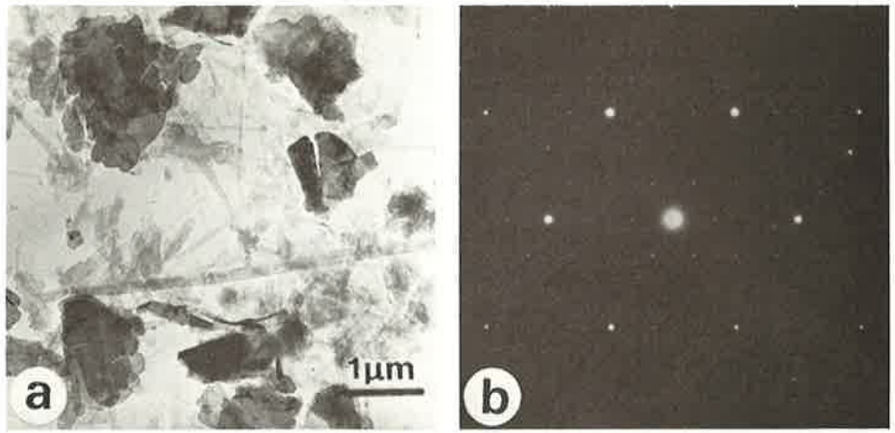

Figure 6.17 (a) Platy subhedral chlorite and thin, lath-like illite. (b) Diffraction pattern from chlorite plate. See Figure 6.11 (b) and (d) for examples of illite diffraction

Usually, they are composed of platy particles with indeterminate shapes yielding similar hexagonal electron-diffraction patterns. A distinction might be made by measuring the 060 reflections (in the case of trioctahedral chlorite and dioctahedral illite) but the difference is very small and cannot always be made with confidence. In some materials, however, chlorite and illite do have quite different morphologies. Figure 6.17 shows a clay fraction containing both minerals, which was separated from a reservoir sandstone. In this instance the illite is in a filamentous or lath-like form, whereas the chlorite occurs in platy, more electron-dense particles. Celadonite and glauconite also tend to occur in short lath-like particles.

6.7.4 *Smectites*

This group of minerals is quite varied morphologically, although most specimens are characterized by extremely fine-grained, poorly defined particles, with diffuse outlines and curled edges.

Montmorillonite typically occurs in this way (Figure 6.18(a)), and yields SAD patterns consisting of continuous or semicontinuous rings (Figure 6.18(b)). Such a pattern is indicative of turbostratic disorder, and shows that the constituent layers of the particle selected are randomly stacked one above the other. Many montmorillonite particles can therefore be regarded as aggregates, and indeed, a foliated, lamellar aggregate structure is often obvious.

Nontronite often shows a lath-like morphology, with the direction of elongation again being the *a*-axis (Figure 6.18(c)), but the mineral can also occur in poorly defined particles, as described at the beginning of this section. Hectorite is another smectite that occurs in *a*-axis-elongated laths.

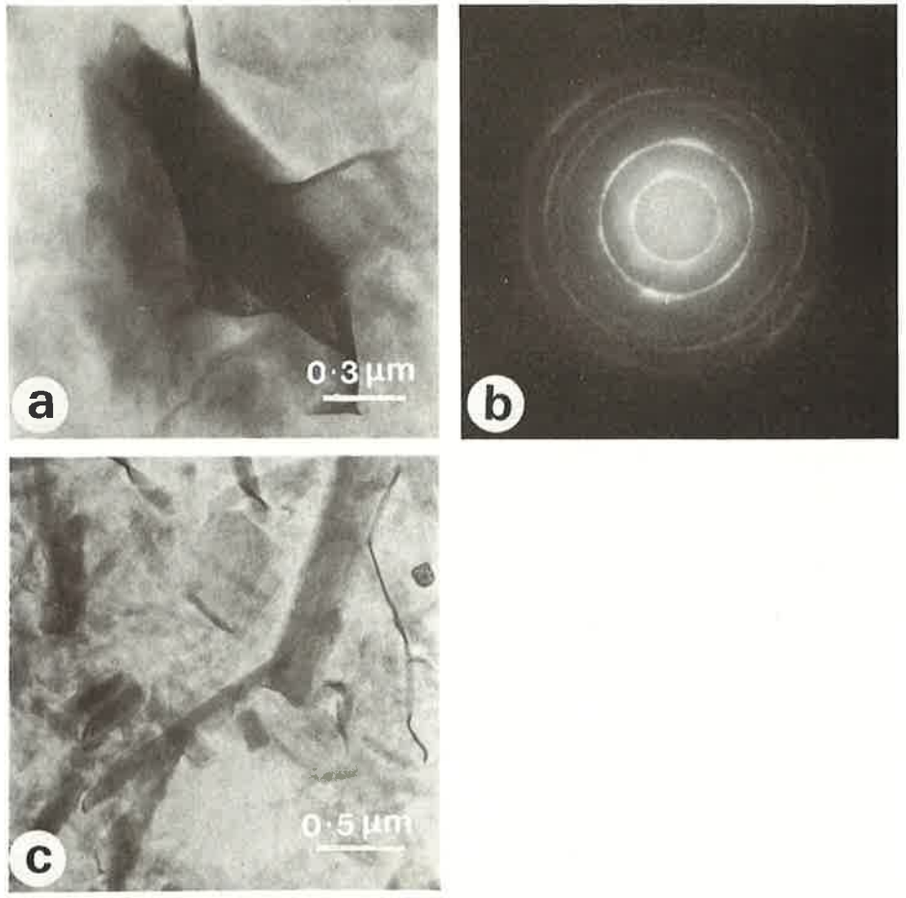

Figure 6.18 (a) Foliated montmorillonite aggregate giving: (b) a ring pattern indicative of turbostratic disorder in stacking of the layers. (c) Lath-like nontronite

Saponite occurs both in isometric, platy particles and in stubby laths aligned along *a* (Figure 6.19(a) and (b)). Electron diffraction often shows evidence of a higher degree of structural order than is found, for example, in montmorillonite. Thus, what appear to be relatively thick particles may yield spotty rather than continuous ring patterns, and single-crystal hexagonal spot patterns also occur (Figure 6.19(c) and (d)). Beidellite also appears to possess greater order than is the norm for smectites.

6.7.5 *Magnesium-rich clays*

In general, these minerals occur in either platy or fibrous forms, the latter being of unquestionable diagnostic value.

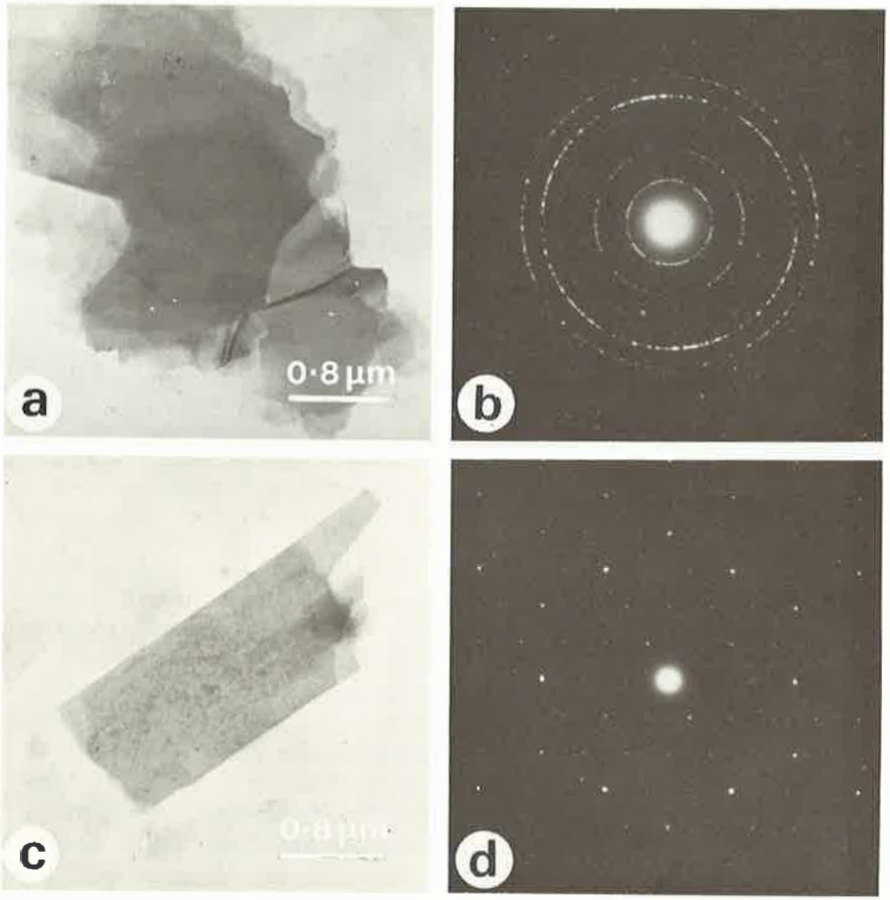

Figure 6.19 (a) and (b) platy saponite aggregate giving incomplete rings or arcs in diffraction. (c) and (d) lath-like saponite with single-crystal spot pattern

Talc is composed of rather thick, well-defined, platy particles that yield the usual, single-crystal hexagonal ED pattern (Figure 6.20(a) and (b)). In contrast, other magnesium-rich phyllosilicate clays such as kerolite, stevensite and swelling chlorite are characterized by a montmorillonite-like morphology and yield diffraction patterns typical of turbostratic disorder.

Palygorskite and sepiolite are both composed of *a*-axis-elongated fibres. The fibrous form in palygorskite is often better developed than that of sepiolite (Figure 6.20(c) and (e)), although this observation may be of little diagnostic value. Both minerals are sensitive to electron-beam damage and care is required in the taking of micrographs. Electron-diffraction patterns show a series of weak layer lines, and on the central line, the characteristic 10.8 and 12 Å spacings of palygorskite and sepiolite respectively can be determined (Figure 6.20(d) and (f)).

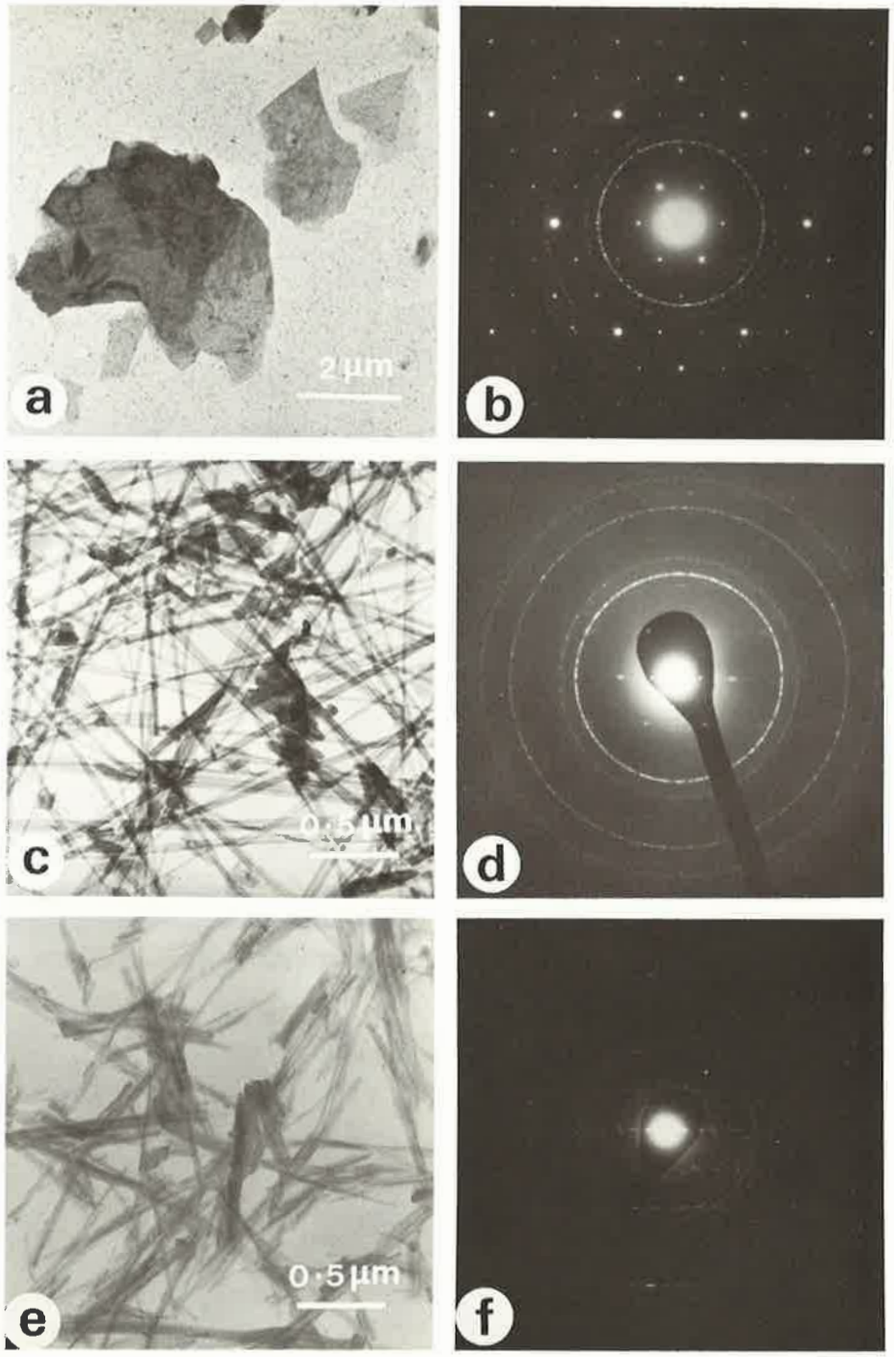

Figure 6.20 (a) Subhedral platy talc particles; (b) talc SAD spot pattern with rings from Al. (c) Palygorskite and (e) sepiolite fibres. Diffraction patterns (d) and (f), respectively, appear similar, apart from different spacing of spots along central row; 10.8 Å for palygorskite and 12 Å for sepiolite. Streaking along layer lines indicates structural disorder; rings are from Al

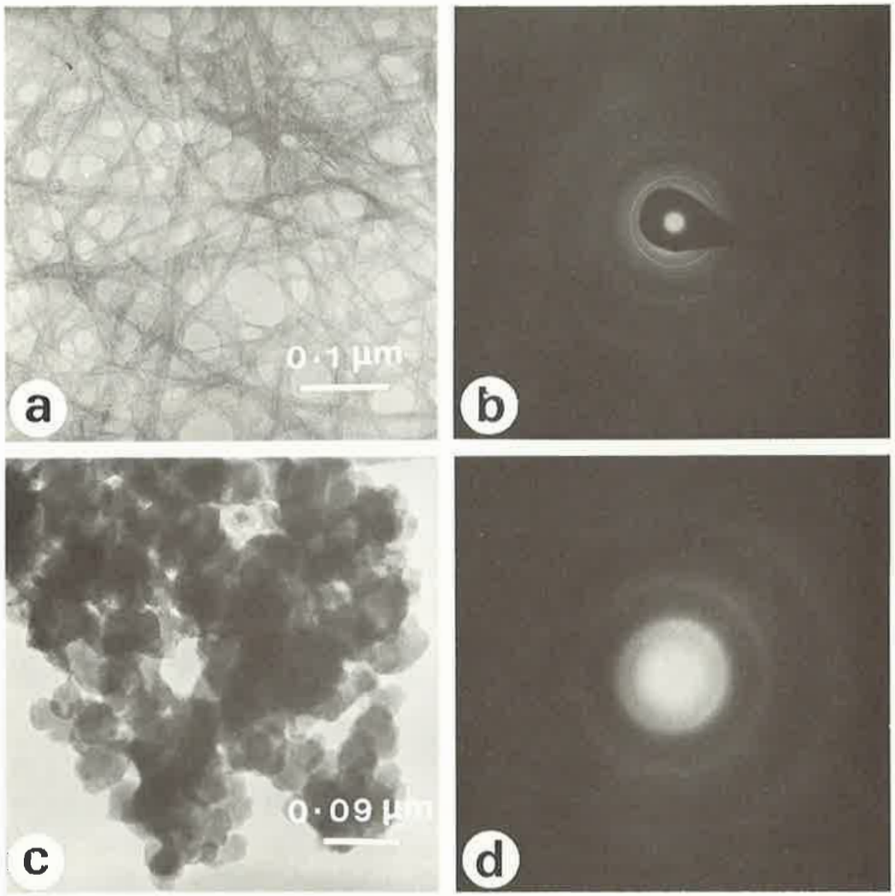

Figure 6.21 (a) and (b) show morphology and diffraction patterns which are quite diagnostic of imogolite; *d*-spacings of rings shown in (b) are from centre outwards: 4.1, 3.8, 3.3, 2.3, 2.1 and 1.4 Å. (c) and (d) allophane appears to be virtually amorphous showing only two very diffuse rings in SAD

6.7.6 *Imogolite and allophane*

Imogolite can be identified unequivocally by electron microscopy, which can be regarded as the most diagnostic method. The mineral consists of a mass of long and exceedingly fine fibres (Figure 6.21(a)). The fibres range in thickness from ~ 100 to 200 Å, but are some microns long. High-resolution micrographs show that the fibres are really bundles of tubes, and bring out a characteristic 'railway-track' appearance. The electron-diffraction patterns vary, according to whether the fibres are randomly oriented or in a parallel alignment, but they can be indexed by taking the fibre direction as the *c*-axis and the interfibre distance as the *b*-axis (Figure 6.21(b)). A reflection corresponding with the

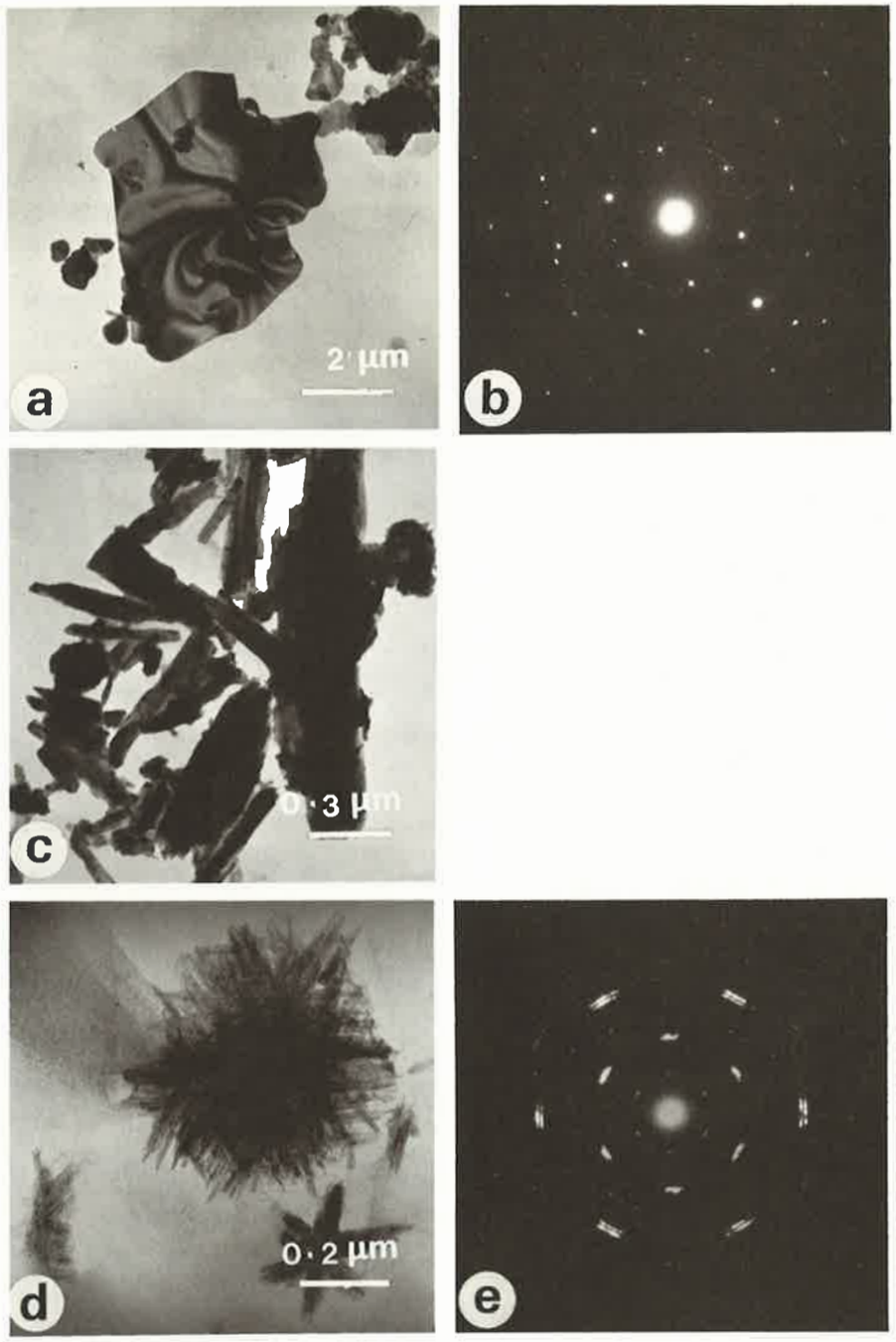

Figure 6.22 (a) Electron-dense platy hematite particle gives hexagonal spot pattern (b), with spacing of 2.5 Å; rings from Al. (c) Stubby lath-like goethite and (d) the more typical, acicular star-shaped goethite particles giving (e) a pseudohexagonal pattern of short arcs due to twinning

intertube distance (23 Å) can be observed, but only for short exposures.

Allophane consists of fine, rounded particles (Figure 6.21(c)), which are sometimes seen to have a ring structure at high magnification. Electron-diffraction patterns are poor, consisting essentially of only two broad ring reflections, yielding spacings at 3.3 and 2.25 Å (Figure 6.21(d)).

6.7.7 *Iron minerals*

These minerals show a range of morphological characteristics, that help to identify them even when they occur as minor components in complex mixtures.

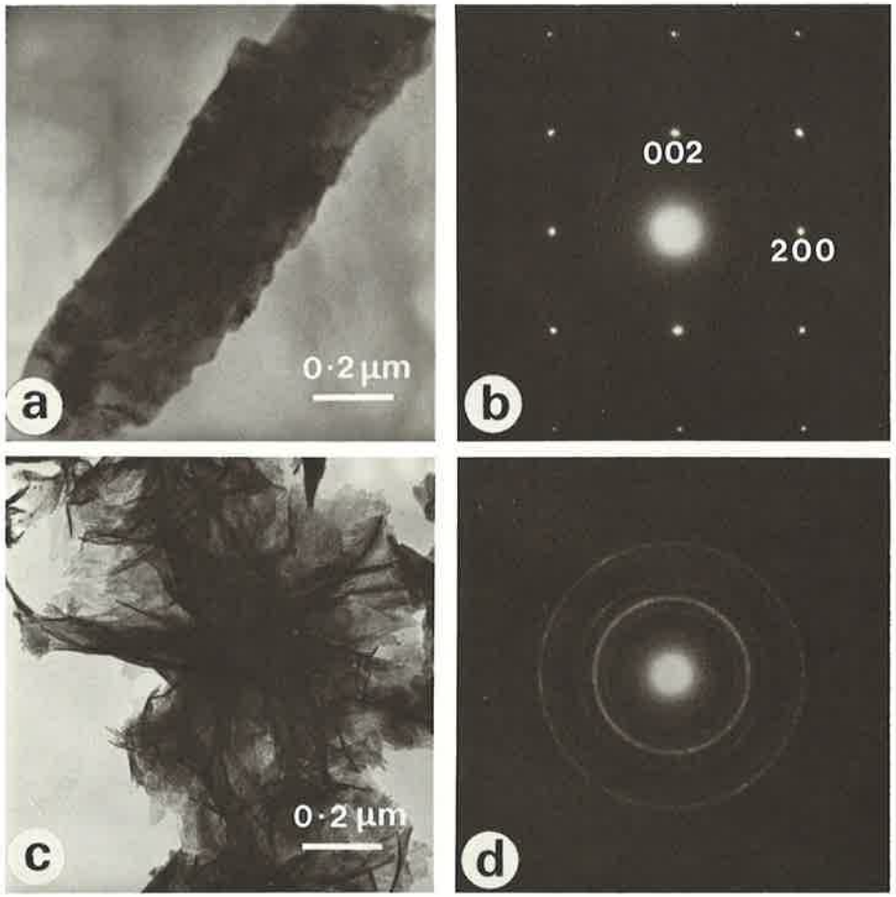

Figure 6.23 (a) Well-crystallized lepidocrocite lath, elongated along *c*-axis. (b) SAD pattern representing the (h0) plane of reflections; rings from Al. (c) Foliated aggregate of poorly crystallized lepidocrocite which can be identified from ring diffraction pattern (d), with *d*-spacings 6.3, 3.0, 2.5, 2.1, 1.6 and 1.5 Å

Hematite commonly occurs as small, electron-dense, platy particles, in a rough hexagonal or subequant shape and with well-defined outlines. Interference effects on the crystal surface are common (Figure 6.22(a)). The electron-diffraction pattern (Figure 6.22(b)) is a single-crystal, hexagonal type, similar to that of the layer silicates. However, measurement of the repeat distance enables hematite to be readily distinguished from all the major clay minerals yielding a spacing of 2.5 Å as opposed to 4.5 Å for the layer silicates.

Goethite tends to occur as poorly developed, lath-like particles elongated along the *c*-axis, and also as star-shaped twin crystals (Figure 6.22(c) and (d)). The ED patterns yielded by these twins are quite characteristic, with hexagonally arranged clusters of slightly arced spots (Figure 6.22(e)). Careful

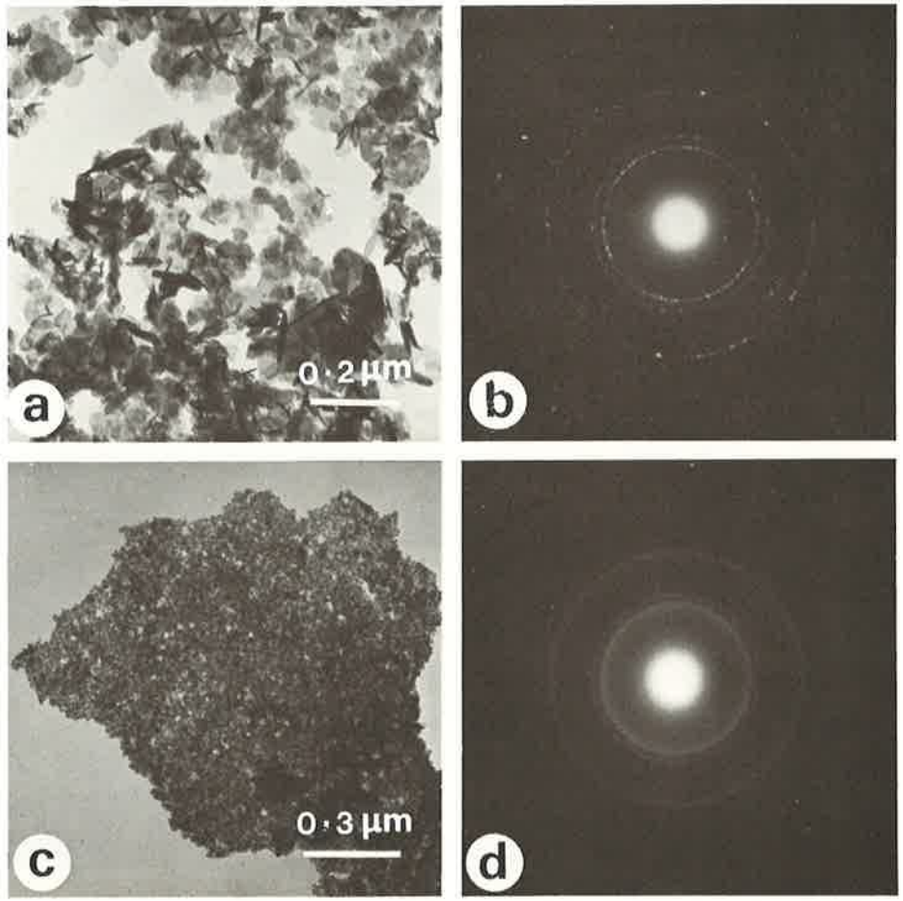

Figure 6.24 (a) and (b) Feroxyhyte. (*c*) and (*d*) ferrihydrite. Note that feroxyhyte usually gives a four-ring pattern with *d*-spacings 2.5, 2.2, 1.7 and 1.5 Å, while ferrihydrite gives a fifth ring at 1.9 Å

measurement of the 111 reflection can be used to determine the amount of Al substitution in the goethite structure.

Lepidocrocite often shows a stubby, *c*-axis-elongated, lath-like form (Figure 6.23(a)), and yields a diffraction pattern displaying a rectangular array of spots (Figure 6.23(b)) from the [010] zone axis, with $d_{200} = 1.55$ Å and $d_{002} = 1.96$ Å. Lepidocrocite also occurs in a poorly crystallized, crumpled sheet form, which shows a characteristic ring-like ED pattern (Figure 6.23(d) and (e)).

Ferrihydrite and feroxyhyte both show a fine-grained, indeterminate morphology, and yield continuous-ring ED patterns (Figure 6.24(a), (b), (c)

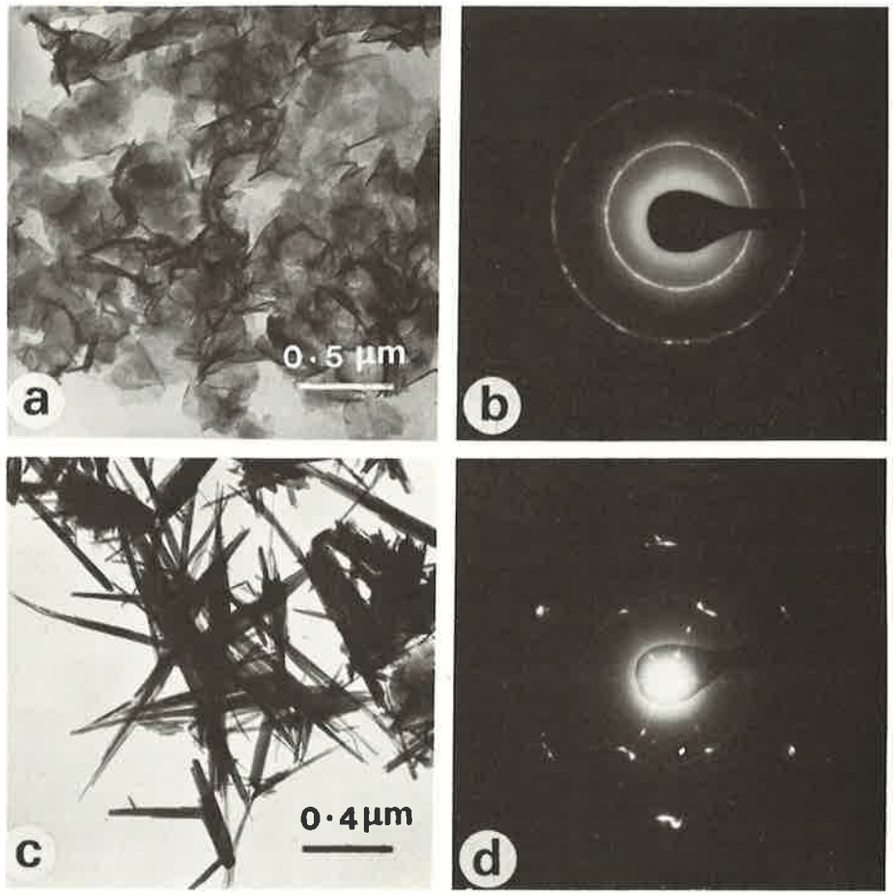

Figure 6.25 (a) and (b) Poorly crystallized vernadite giving only two diffraction rings at 2.5 and 1.4 Å. (c) Cryptomelane type of material, identified from diffraction pattern (d), with closest spaced row of spots of 6.9 Å

and (d)). Measurement of these rings yields the same series of spacings recorded by X-ray diffraction, so that the ED pattern is quite diagnostic.

6.7.8 *Manganese minerals*

These minerals may be very difficult to identify by XRD when they occur in clay materials. Their identification by electron microscopy is now a rapidly developing field, the two examples shown next merely illustrating the potential of the method.

Vernadite is an example of a very poorly crystalline phyllomanganate, and is characterized by thin, crumpled sheets which yield a ring ED pattern with characteristic spacings at 2.5 and 1.4 Å. (Figure 6.25(a) and (b)).

Cryptomelane by contrast, is a well-crystallized tectomanganate and shows a distinct acicular form. SAD patterns from a star-shaped twin show streaked rows of spots from each component crystal, with a *d*-spacing of 6.9 Å. (Figure 6.25(c) and (d)).

6.7.9 *Silica minerals*

Quartz is not easily studied by the TEM, since it rarely occurs in sufficiently small particles. In addition, the absence of any particular cleavage plane makes it difficult to characterize the mineral by electron diffraction.

The tridymite-like mineral that occurs in clays has a platy morphology (Figure 6.26(a)), with individual particles ranging from 0.1 μm to greater than 1 μm in diameter, depending on the nature of the occurrence. The SAD pattern

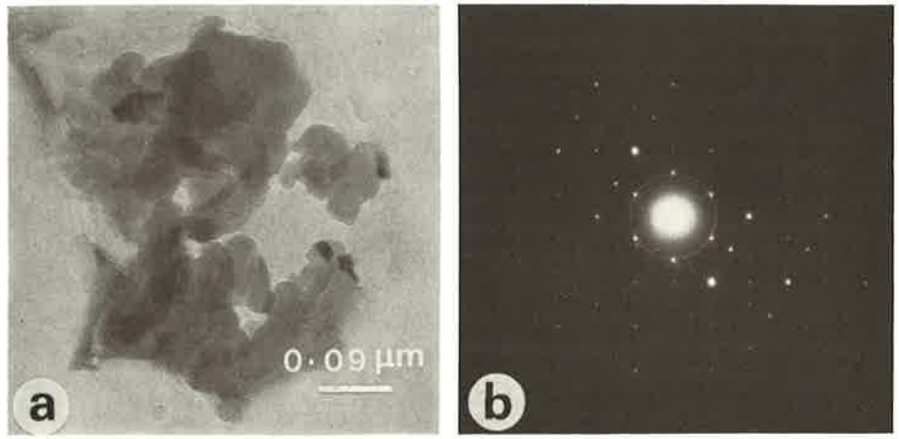

Figure 6.26 (a) Small platy tridymite crystals, (b) SAD pattern shows hexagonal array of spots with strong streaking between reflections, indicating disorder of the structure. Diffracting rings here are from montmorillonite

(Figure 6.26(b)) from individual flakes yields a hexagonal array of spots with *d*-spacing of 8.64 Å, and also shows strong streaking between the reflections. This pattern is indicative of disordered α-tridymite (Wilson *et al.*, 1974).

References

Agar, A.W. (1978) 'Operation of the electron microscope', in *Principles and Practice of Electron Microscope Operation*, (A.W. Agar, R.H. Alderson and D. Chescoe eds.), North-Holland, Amsterdam, 166–190.

Anderson, K. (1968) An image intensifier for the electron microscope, *J. Sci. Instr. (J. Phys. E)* **Ser. 2, 1**, 601–603.

Bates, T.F. (1971) 'The kaolin minerals', in *The Electron-Optical Investigation of Clays*, (J.A. Gard ed.) Mineralogical Society, London, 109–157.

Beutelspacher, H. and van der Marel, H.W. (1968) *Atlas of Electron Microscopy of Clay Minerals and their Admixtures*. Elsevier, Amsterdam, 333 pp.

Bresson, L.-M. (1981) Ion micromilling applied to the ultra-microscopic study of soils. *Soil Sci. Soc. Am. J.*, **45**, 568–573.

Brindley, G.W. and De Kimpe, C. (1961) Identification of clay minerals by single crystal diffraction. *Am. Mineral.*, **46**, 1005–1016.

Comer, J.J. (1971) 'Specimen preparation', in *The Electron-Optical Investigation of Clays*, (J.A. Gard ed.) Mineralogical Society, London, 79–108.

Conley, R.F. (1966) Statistical distribution of particle size and shape in the Georgia kaolins. *Clays & Clay Miner.*, **14**, 317–330.

Eitel, W. and Gotthardt, E. (1940) Der Einfluß von Elektroneninterferenzen auf die Abbildung von Kristallen im Ubermikroskop. *Naturwissenschaften*, **28**, 367.

Farmer, V.C., Russell, J.D. and Berrow, M.L. (1980) Imogolite and proto-imogolite allophane in spodic horizons: evidence from a mobile aluminium silicate complex in podzol formation. *J. Soil Sci.*, **80**, 673–684.

Gard, J.A. (1971) *The Electron-Optical Investigation of Clays*, Mineralogical Society, London, 383 pp.

Grim, R.E. and Güven, N. (1978) *Bentonites: Geology, Mineralogy, Properties and Uses* (*Dev. Sedimentol.*, **24**) Elsevier, Amsterdam, 256 pp.

Hirsch, P.B., Howie, A., Nicholson, R.B., Pashley, D.W. and Whelan, N.J. (1965) *Electron Microscopy of Thin Crystals*, Butterworth, London, 549 pp.

Iijima, S. and Buseck, P.R. (1978) Experimental study of disordered mica structures by high-resolution electron microscopy. *Acta Crystallog.*, **A34**, 709–719.

Mackenzie, R.C., Follett, E.A.C. and Meldau, R. (1971) 'The oxides of iron, aluminium, and manganese,' in *The Electron-Optical Investigation of Clays*, (J.A. Gard ed.), Mineralogical Society, London, 315–344.

Méring, J. and Oberlin, A. (1971) The smectites. In *The Electron-Optical Investigation of Clays*, (J.A. Gard ed.), Mineralogical Society, London, 193–229.

Nadeau, P.H. (1985) The physical dimensions of fundamental clay particles. *Clay Miner.*, **20**, 499–514.

Nadeau, P.H., Tait, J.M., McHardy, W.J. and Wilson, M.J. (1984a) Interstratified XRD characteristics of physical mixtures of elementary clay particles. *Clay Miner.*, **19**, 67–76.

Nadeau, P.H., Wilson, M.J., McHardy, W.J. and Tait, J.M. (1984b) Interparticle diffraction: a new concept for interstratified clays. *Clay Miner.*, **19**, 757–769.

Nadeau, P.H., Wilson, M.J., McHardy, W.J. and Tait, J.M. (1985) The conversion of smectite to illite during diagenesis: evidence from some bentonites and sandstones. *Miner. Mag.*, **49**, 393–400.

Paulus, M., Dubon, A. and Etienne, J. (1975) Application of ion-thinning to the study of the structure of argillaceous rocks by transmission electron microscopy. *Clay Miner.*, **10**, 417–426.

Reid, N. (1975) 'Ultramicrotomy', in *Practical Methods in Electron Microscopy*, 3. II (A.M. Glauert ed.) North-Holland, Amsterdam.

Robertson, R.H.S., Brindley, G.W., and Mackenzie, R.C. (1954) Mineralogy of the kaolin clays from Pugu, Tanganyika. *Am. Mineral.*, **39**, 118–139.

Ruska, H. (1943) Ubermikroskopische Untersuchungen an Asbeststaub und Asbestlungen, *Arch. Gewerbepath., Gewerbehyg.*, **11**, 575–578.

Smart, P. and Tovey, N.K. (1981) *Electron Microscopy of Soils and Sediments: Examples*, Clarendon Press, Oxford, 178 pp.

Smart, P. and Tovey, N.K. (1982) *Electron Microscopy of Soils and Sediments: Techniques*, Clarendon Press, Oxford, 400 pp.

Spurr, A.R. (1969) A low-viscosity epoxy resin embedding medium for electron microscopy. *J. Ultrastruct. Res.*, **26**, 31.

Smith, B.F.L. (1984) The determination of silicon in ammonium oxalate extract of soils. *Comm. Soil Sci. & Pl. Anal.*, **15**, 199–204.

Steeds, J.W. (1979) 'Convergent beam electron diffraction,' in *Introduction to Analytical Electron Microscopy*, (J.J. Hren, J.I. Goldstein, and D.C. Jay eds.), Plenum Press, New York, 387–422.

Sudo, T., Shimoda, S., Yotsumito, H. and Acta, S. (1981) *Electron Micrographs of Clay Minerals.* (*Dev. Sedimentol.*, **31**) Elsevier, Amsterdam, 203 pp.

Tokiwai, M., Moriguchi, S., Shinkawa, T., and Watanabe, E. (1983) Automatic computer analysis of electron diffraction patterns. *JEOL News*, **21E(2)**, 2–6.

Vainshtein, B.K. (1964) *Structure Analysis by Electron Diffraction*, Pergamon Press, Oxford, 420 pp.

Walker, G.F. (1967) Chemical exfoliation of vermiculite and the production of colloidal dispersions. *Science*, **156**, 385–387.

Wilson, M.J., Russell, J.D. and Tait, J.M. (1974) A new interpretation of the structure of disordered α-cristobalite. *Contrib. Miner. & Petrol.*, **47**, 1–6.

Yada, K. (1967) Study of chrysotile by a high resolution microscope. *Acta Crystallog.*, **23**, 704–707.

Yariv, S. and Cross, H. (1979) *Geochemistry of Colloidal Systems*, Springer-Verlag, Berlin, 450 pp.

Yoshida, T. (1973) Elementary layers in the interstratified clay minerals as revealed by electron microscopy. *Clays & Clay Miner.*, **21**, 413–420.

Zvyagin, B.B. (1967) *Electron-Diffraction Analysis of Clay Mineral Structures*, Plenum Press, New York, 364 pp.